

Low and High Energy Limits of Particle Spectra in QCD Jets

Sergio Lupia* and Wolfgang Ochs†

*Max-Planck-Institut für Physik, (Werner-Heisenberg-Institut)
Föhringer Ring 6, 80805 München, Germany*

Abstract

Charged particle energy spectra in e^+e^- annihilation are compared with the analytical predictions from the QCD evolution equation in the Modified Leading Log Approximation. With the nonperturbative initial condition shifted down to threshold as suggested by the Local Parton Hadron Duality picture a good description of the data from the lowest up to highest available energies results. The two essential parameters in this approach are determined from a moment analysis. The sensitivity of the fit to the running of α_s and to the number of active flavours (including a light gluino) is demonstrated. For very high energies the theory predicts a scaling behaviour in certain rescaled variables (“ ζ -scaling”). The data show an approximate behaviour of this type in the present energy range and come close to the predicted asymptotic scaling function for the small particle energies.

*E-mail address: lupia@mppmu.mpg.de

†E-mail address: wwo@mppmu.mpg.de

1 Introduction

The perturbative QCD describes well the properties of hard processes. The problem of the soft limit of the perturbation theory and the transition to the hadronic final state, however, is still not solved at a fundamental level. The studies of the global properties of the hadronic final states gave support to the idea that the colour confinement mechanism should be rather soft [1,2]. Meanwhile, the close similarity between hadronic and partonic final states has been found for a large variety of observables, provided the parton cascade in the perturbative calculation is evolved down to rather low virtualities of the order of a few hundred MeV; this phenomenon is called “Local Parton Hadron Duality” (LPHD) [3] (for a recent review, see [4]).

An interesting prediction concerns the momentum spectrum of the particles in a jet at very high energies, namely the approximately Gaussian distribution in the variable $\xi = \ln(P_{\text{jet}}/p_{\text{hadron}})$, the so-called “hump backed plateau” [5,6,7], with a suppression of low momentum particles following from the soft gluon interference [8,9].

Within the LPHD picture, not only the very high energy behaviour of the spectrum is considered. Rather, one starts from the initial condition near threshold for the parton cascade where only one parton is present and derives the distribution at higher energies using the appropriate QCD evolution equation. In this case – apart from the overall normalization – the theory has only two essential parameters, the QCD scale Λ in the running coupling (at the one loop level) and a cut-off Q_0 in the transverse momentum of the gluon emission. In the Double Logarithmic Approximation (DLA) one takes into account the leading contributions from the collinear and soft singularities which dominate at very high energies and determine the asymptotic behaviour of the observables. At present energies the next-to-leading corrections of relative order $\sqrt{\alpha_s}$ are important and are fully taken into account in the Modified Leading Logarithmic Approximation (MLLA). An explicit analytical expression for the particle energy distribution is found in this approximation for the special case $Q_0 = \Lambda$, the so-called limiting spectrum [3]. Remarkably, the experimental momentum spectra in the PETRA [10] and LEP [11] energy range gave support to the perturbative predictions [3], and this success has been continued recently to the higher energies at LEP-1.5 ([12,13,14] and [15]) and the TEVATRON [16].

The energy evolution of the spectrum and its connection to the initial condition at threshold is most conveniently studied using the moment representation of the spectrum. Recently, the first such moment analysis, based on the analytical results [17], has been performed over the full cms energy range available in e^+e^- annihilation [18]. There are a number of advantages

of the moment analysis over the analysis of the spectrum itself: (a) there are analytical formulae which keep the two essential parameters of the theory Q_0 and Λ independent [17], whereas explicit formulae for the spectrum are only available for the limiting case $Q_0 = \Lambda$; (b) the moments evolve with energy independently of each other. Their absolute size is determined by the initial condition at the threshold of the process; (c) the moments of order $q \geq 1$ are independent of the overall normalization and depend only on the two essential parameters of the LPHD approach; (d) the difference between the theory with running coupling and an artificial theory with fixed coupling can be studied directly and (e) the flavour thresholds can be included in the theoretical calculations. As the calculations of the moments include the soft part of the spectrum, the mass effects have to be taken into account.

Having studied the behaviour of the spectrum towards low energies it is also interesting to study the limiting behaviour of the spectrum for very high energies as the theories typically predict simple asymptotic expressions or a characteristic scaling behaviour. Then one can investigate to what extent this behaviour appears already at available energies. The asymptotic behaviour of the QCD jet is obtained in the DLA. There is indeed a finite scaling limit in certain rescaled variables and the scaling function can be calculated [20].

The purpose of this paper is twofold. First, we present more details of our previous moment analysis [18] (see also [19]) as well as further results concerning all points (a) – (e) above. Secondly, we give the description of the shape of the spectrum and discuss the approach to the asymptotic limit in the appropriate scaling variables.

2 Theoretical description of particle spectra

2.1 Evolution equations

The multiparticle properties of a QCD jet is conveniently described by the generating functional $Z(\kappa, Q_0, \{u(k)\})$. The arguments are the hardness scale κ of the jet, which is defined in terms of jet momentum P and opening angle Θ by

$$\kappa = 2P \sin \frac{\Theta}{2} \approx P\Theta \quad (1)$$

where the approximation holds for small angles; Q_0 is the lower cut-off in the transverse momentum of the emitted parton

$$k_{\perp} \geq Q_0. \quad (2)$$

The inclusive densities can be obtained by functional differentiation of Z over the probing functions $u(k)$ referring to parton momentum k . Our analysis is based on the evolution equation for the gluon jet as discussed in [17]. We rederive here the basic equations for the energy spectrum whereby we start from the evolution equation of the generating functional and show the various steps of the approximations.

The evolution of the generating functional with the hardness scale κ is given by the ‘‘Master Equation’’ [2,21]

$$\begin{aligned} \frac{d}{d \ln \kappa} Z_A(\kappa, Q_0) &= \frac{1}{2} \sum_{B,C} \int_0^1 dz \\ &\times \frac{\alpha_s(k_\perp^2)}{2\pi} \Phi_A^B(z) [Z_B(z\kappa, Q_0) Z_C((1-z)\kappa, Q_0) - Z_A(\kappa, Q_0)]. \end{aligned} \quad (3)$$

This equation describes the evolution of the jet by the splitting of the primary parton A into partons B and C at reduced scales $z\kappa$ and $(1-z)\kappa$; $\Phi_A^B(z)$ denote the DGLAP splitting functions. The integral over the secondary energy fraction z has to respect the limits (2) for the transverse momentum $k_\perp = z(1-z)\kappa$.

The Master Equation (3) yields results complete within the MLLA at high energies. Furthermore, the energy conservation constraints are taken into account. Because of (2) the evolution starts at $\kappa = Q_0$. Then the initial condition for solving this system of equations reads

$$Z_A(\kappa, Q_0; \{u\})|_{\kappa=Q_0} = u_A(k = P) \quad (4)$$

which means that there is only one parton in the cascade at threshold.

The solution of the evolution equation (3) together with the boundary condition (4) yields perturbative expansions in α_s in all orders, which for many observables can be resummed and exponentiate at high energies. The MLLA takes into full account the leading and next-to-leading contributions in the expansion of $\sqrt{\alpha_s}$ in the exponent at high energies.

To this accuracy one can actually neglect the energy recoil and replace the $1-z$ by 1 in the arguments of Z and furthermore neglect the z -dependence of Z and of $\alpha_s(k_\perp(z))$ in the regular z -integrals. With these simplifications one obtains a simplified form of (3), the MLLA master equation [21].

The evolution equation for the single inclusive density in the secondary parton energy k is obtained from Z by functional differentiation

$$D(k, \kappa, Q_0) = \frac{\delta}{\delta u(k)} Z(\kappa, Q_0, \{u\})|_{u=1}. \quad (5)$$

After differentiation (5) of the MLLA master equation [21] we obtain the evolution of the parton densities in quark and gluon jets

$$\begin{aligned}\frac{d}{d \ln \kappa} D_g(k, \kappa) &= \int_x^1 \frac{dz}{z} \gamma_0^2(z\kappa) D_g(k, \kappa) \\ &\quad + \gamma_0^2(\kappa) \left(-\frac{11}{12} D_g(k, \kappa) + \frac{T_R n_f}{3N_C} [2D_q(k, \kappa) - D_g(k, \kappa)] \right) \\ \frac{d}{d \ln \kappa} D_q(k, \kappa) &= \frac{C_F}{N_C} \left(\int_x^1 \frac{dz}{z} \gamma_0^2(z\kappa) D_g(k, \kappa) - \frac{3}{4} \gamma_0^2(\kappa) D_g(k, \kappa) \right)\end{aligned}\quad (6)$$

Here $x = k/P$, n_f and N_C denote the number of flavours and colours respectively, $C_F = \frac{N_C^2 - 1}{2N_C}$ and $T_R = \frac{1}{2}$. The anomalous multiplicity dimension γ_0 is given in one-loop approximation by

$$\gamma_0^2(k_\perp) = \frac{2N_C \alpha_s(k_\perp)}{\pi} = \frac{4N_C}{b \ln(k_\perp/\Lambda)}, \quad b = \frac{11}{3} N_C - \frac{2}{3} n_f. \quad (7)$$

The initial conditions for these evolution equations follow from (4)

$$D_A(k, \kappa)|_{\kappa=Q_0} = \delta(k - P_A) \quad , \quad A = q, g \quad (8)$$

It is convenient to write these equations in logarithmic variables, namely

$$\begin{aligned}Y = \ln \frac{\kappa}{Q_0} &\approx \ln \frac{P\Theta}{Q_0}, & \xi = \ln \frac{1}{x} = \ln \frac{P}{k}, & \lambda = \ln \frac{Q_0}{\Lambda}, \\ \xi' = \ln \frac{zP}{k} &= \xi + \ln z, & y' = \ln \frac{zP\Theta}{Q_0} &= Y + \ln z.\end{aligned}\quad (9)$$

Then, after redefining $D(k, P, \Theta) \rightarrow D(\xi, Y)$ and $D(k, zP, \Theta) \rightarrow D(\xi', y')$ we obtain after integration of (6) with (8)¹

$$\begin{aligned}D_g(\xi, Y) &= \delta(\xi) + \int_0^\xi d\xi' \int_0^{Y-\xi} dy' \gamma_0^2(y' + \xi') D_g(\xi', y' + \xi') \\ &\quad + \int_\xi^Y dy \gamma_0^2(y) \left(-\frac{11}{12} D_g(\xi, y) + \frac{T_R n_f}{3N_C} [2D_q(\xi, y) - D_g(\xi, y)] \right) \\ D_q(\xi, Y) &= \delta(\xi) + \frac{C_F}{N_C} \left(\int_0^\xi d\xi' \int_0^{Y-\xi} dy' \gamma_0^2(y' + \xi') D_g(\xi', y' + \xi') \right. \\ &\quad \left. - \frac{3}{4} \int_\xi^Y dy \gamma_0^2(y) D_g(\xi, y) \right).\end{aligned}\quad (10)$$

¹We use here the same notation for both densities $D(k) = dn/dk$ and $D(\xi) = dn/d\xi = kdn/dk$.

The double integral terms in these equations originate from the singular parts of the splitting functions $\Phi(z) \sim 1/z$ and represent the leading double logarithmic terms of the DLA, the single integrals include the MLLA corrections from the finite parts of the splitting functions within the required approximation. In the DLA the spectra in quark and gluon jets are related by

$$D_q(\xi, Y) - \delta(\xi) = \frac{C_F}{N_C}(D_g(\xi, Y) - \delta(\xi)) \quad (11)$$

Replacing D_q by its leading order contribution $\frac{C_F}{N_C}D_g$ in the nonleading term of eq. (10) for D_g , we obtain the integral evolution equation for D_g

$$D_g(\xi, Y) = \delta(\xi) + \int_0^\xi d\xi' \int_0^{Y-\xi} dy' \gamma_0^2(y' + \xi') D_g(\xi', y' + \xi') - \frac{a}{4N_C} \int_\xi^Y dy \gamma_0^2(y) D_g(\xi, y) \quad (12)$$

with $a = \frac{11}{3}N_C + \frac{2n_f}{3N_C^2}$. The corresponding differential equation reads

$$\left(\frac{\partial}{\partial \xi} + \frac{\partial}{\partial Y} \right) \frac{\partial D_g(\xi, Y, \lambda)}{dY} - \gamma_0^2(Y) D_g(\xi, Y, \lambda) = -a \left(\frac{\partial}{\partial \xi} + \frac{\partial}{\partial Y} \right) \left(\frac{\gamma_0^2(Y)}{4N_C} D_g(\xi, Y, \lambda) \right). \quad (13)$$

For $a = 0$ it corresponds to the DLA. In order to solve this equation one can introduce the Laplace transform ($D \equiv D_g$)

$$D(\xi, Y) = \int_{\tau-i\infty}^{\tau+i\infty} \frac{d\omega}{2\pi i} e^{\omega\xi} D_\omega(Y), \quad (14)$$

where the integral runs parallel to the imaginary axis to the right of all singularities of the integrand in the complex ω -plane. Then $D_\omega(Y)$ fulfils the ordinary linear differential equation

$$\left(\omega + \frac{d}{dY} \right) \frac{d}{dY} D_\omega(Y, \lambda) - \gamma_0^2(Y) D_\omega(Y, \lambda) = -a \left(\omega + \frac{d}{dY} \right) \frac{\gamma_0^2(Y)}{4N_C} D_\omega(Y, \lambda). \quad (15)$$

This is the basic equation used in [17] to derive the parton distributions and their moments for gluon jets. For quark jets the high energy approximation

$D_q = \frac{C_F}{N_C} D_g$ is taken. The differential equation (13) has also been analyzed in [18].

One approach towards a solution of this equation is based on the anomalous dimension ansatz

$$D_\omega(Y, \lambda) = D_\omega(Y_0, \lambda) \exp \left(\int_{Y_0}^Y dy \gamma_\omega[\alpha_s(y + \lambda)] \right) \quad (16)$$

which yields a differential equation for γ_ω with two solutions, one of which dominating at high energies. Alternatively, one can find the solution of (15) directly in terms of hypergeometric functions [17,2].

2.2 Moments of parton distributions

There are various advantages of studying the moments of the parton distributions as discussed in the Introduction. Analytical predictions for QCD jets have been presented in [7,17].

2.2.1 Definitions and evolution equation

The unnormalized moments \mathcal{M}_q of the ξ -distribution are defined by

$$\mathcal{M}_q(Y, \lambda) = \int_0^Y d\xi \xi^q D(\xi, Y, \lambda) \quad (17)$$

with \mathcal{M}_0 equal to the average parton multiplicity $\bar{\mathcal{N}}$. They are closely related to the Laplace transform

$$D_\omega(Y, \lambda) = \int_0^Y d\xi e^{-\xi\omega} D(\xi, Y, \lambda), \quad (18)$$

by

$$\mathcal{M}_q = (-1)^q \frac{\partial^q}{\partial \omega^q} D_\omega(Y, \lambda)|_{\omega=0}. \quad (19)$$

The moments $\langle \xi^q \rangle$ of the ξ -distribution are then defined by

$$\langle \xi^q(Y, \lambda) \rangle = \frac{\mathcal{M}_q}{\bar{\mathcal{N}}}. \quad (20)$$

One also introduces the cumulant moments $K_q(Y, \lambda)$; the moments of lowest order in q are given by

$$\begin{aligned} K_1 &= \langle \xi \rangle \equiv \bar{\xi}, & K_2 &= \sigma^2 = \langle (\xi - \bar{\xi})^2 \rangle, \\ K_3 &= \langle (\xi - \bar{\xi})^3 \rangle, & K_4 &= \langle (\xi - \bar{\xi})^4 \rangle - 3\sigma^4. \end{aligned} \quad (21)$$

The reduced cumulants are defined by $k_q \equiv K_q/\sigma^q$, in particular the skewness $s = k_3$ and the kurtosis $k = k_4$. The cumulants K_q of general order q can be derived from the expansion:

$$\ln D_\omega(Y, \lambda) = \sum_{q=0}^{\infty} K_q(Y, \lambda) \frac{(-\omega)^q}{q!} \quad (22)$$

and therefore

$$K_q(Y, \lambda) = \left(-\frac{\partial}{\partial \omega} \right)^q \ln D_\omega(Y, \lambda) \Big|_{\omega=0}. \quad (23)$$

At high energies one term of the type (16) dominates and one finds

$$K_q(Y, \lambda) = K_q(0, \lambda) + \int_0^Y dy \left(-\frac{\partial}{\partial \omega} \right)^q \gamma_\omega[\alpha_s(y + \lambda, n_f)] \Big|_{\omega=0} \quad (24)$$

where the evolution starts at $Y = 0$ according to the LPHD picture.

The moments can be obtained via eq. (19) from the evolution equation for D_ω with the appropriate boundary conditions at threshold. These are obtained from the Master Equation (3) with (4) and (5) as

$$\begin{aligned} \overline{\mathcal{N}}(0) &= 1, & \overline{\mathcal{N}}'(0) &= 0 \\ < \xi^q(0) > &= 0 & < \xi^{q'}(0) > &= 0 \quad \text{for } q \geq 1. \end{aligned} \quad (25)$$

On the other hand, the boundary conditions implied by eqs. (10) and (12) are different in case of the multiplicity $\overline{\mathcal{N}}$ because of the approximations involved in this integral equation, whereas they remain the same for the higher moments. For $\lambda > 0$ we find

$$\overline{\mathcal{N}}(0) = 1 \quad , \quad \overline{\mathcal{N}}'(0) = -\frac{B}{\lambda} < 0. \quad (26)$$

The corresponding result is also obtained for D_ω in [17]. This yields a minimum of the multiplicity above threshold with an unphysical value $\overline{\mathcal{N}}(Y_m) < 1$. In case of the limiting spectrum with $\lambda = 0$ both the position in Y and the value of the minimum of the multiplicity $\overline{\mathcal{N}}$ tends to zero and one obtains the boundary conditions $\overline{\mathcal{N}}(0) = 0$ and $\overline{\mathcal{N}}'(0) > 0$ [17]. These problems can be traced back to the approximations in the second integrals in (10) and (12): the correct limits (25) would be obtained, for example, using the modifications (ϵ -terms) proposed in[21].

It should also be noted that the limit $\lambda \rightarrow 0$ is only possible because of these approximations. Otherwise, whereas the energy dependence of the

multiplicity $\overline{\mathcal{N}} \sim \exp(c\sqrt{Y + \lambda})$ has a smooth limit for $\lambda \rightarrow 0$, the absolute normalization (the prefactor) would diverge for $\lambda \rightarrow 0$. This can be seen, for example, in the DLA from (52) with $B = 0$. It will be interesting to study the effect of these approximations in more detail. The subsequent analysis is based on the approximate eqs. (12) and (15) with the corresponding boundary conditions.

2.2.2 Moments for running coupling α_s

The results obtained from the full solution of (15) can be written for arbitrary parameters Q_0 and Λ as:

$$\langle \xi^q \rangle = \frac{1}{\overline{\mathcal{N}}} \sum_{k=0}^q \binom{q}{k} (N_1 L_k^{(q)} + N_2 R_k^{(q)}) \quad (27)$$

where N_1 , N_2 , $L_k^{(q)}$ and $R_k^{(q)}$ are known functions of a , b , $Y + \lambda$ and λ whose explicit expression depends on the order q [17] (see Appendix A1). For the special case of the limiting spectrum, where the two parameters Q_0 and Λ coincide (i.e. $\lambda = 0$), the expressions simplify and all moments can be expressed in terms of the parameter $B \equiv a/b$ and the variable $z \equiv \sqrt{16N_c Y/b}$. The general result for the q -order moments is then the following [17]:

$$\frac{\langle \xi^q \rangle}{Y^q} = P_0^{(q)}(B + 1, B + 2, z) + \frac{2 I_{B+2}(z)}{z I_{B+1}(z)} P_1^{(q)}(B + 1, B + 2, z) \quad (28)$$

where $P_0^{(q)}$ and $P_1^{(q)}$ are polynomials of order $2(q - 1)$. Expanding the Bessel functions and $P_i^{(q)}$, one obtains a series in $1/\sqrt{Y}$. The leading and next-to-leading order results in this expansion (see also [7]) determine the high energy behaviour; the remaining part of the series however is still numerically sizeable at LEP energies (10% contribution to $\bar{\xi}$ and σ^2) and increases towards lower energies. We therefore included the full result (28), also for $P_i^{(q)}$ (for the explicit expressions, see Appendix A2). The average multiplicity of partons is given in this approximation by:

$$\overline{\mathcal{N}}_{LS} = \Gamma(B) \left(\frac{z}{2}\right)^{1-B} I_{B+1}(z). \quad (29)$$

2.2.3 Moments for fixed coupling α_s

In this case the differential equations (13) and (15) can be solved exactly [18]. For D_ω one finds

$$D(\omega, Y) = \left(\frac{\omega/2 + \eta}{\tilde{\omega}} \sinh(\tilde{\omega}Y) + \cosh(\tilde{\omega}Y) \right) e^{-(\omega/2 + \eta)Y} \quad (30)$$

where $\tilde{\omega} = \sqrt{(\omega/2 - \eta)^2 + \gamma_0^2}$. Differentiation (19) yields the moments in the form

$$\overline{\mathcal{N}}_{fix} = \left[\cosh(\bar{\gamma}_0 Y) + \frac{\eta}{\bar{\gamma}_0} \sinh(\bar{\gamma}_0 Y) \right] \exp(-\eta Y) \quad (31)$$

$$\langle \xi_{fix}^q \rangle = [A_q \cosh(\bar{\gamma}_0 Y) + B_q \sinh(\bar{\gamma}_0 Y)] \frac{\exp(-\eta Y)}{\overline{\mathcal{N}}_{fix}} \quad (32)$$

$$\bar{\gamma}_0 \equiv \sqrt{\gamma_0^2 + \eta^2} \quad \eta = \frac{a\gamma_0^2}{8N_C} = \frac{a\alpha_s}{4\pi}$$

The coefficients A_q , B_q are polynomials of order q in Y , given for $q \leq 4$ in the Appendix A3. For $\eta = 0$, one obtains back the DLA results, especially $\overline{\mathcal{N}}_{fix} = \cosh(\gamma_0 Y)$.

These results are obtained using the original boundary conditions, eq. (25). As pointed out above, from the MLLA equation (12) the boundary conditions (26) are obtained. We have also studied the results following from these other boundary conditions: in this case the moments would be shifted towards larger Y at most by 1 unit and the overall description of the data would become worse.

At high energies the results (32) greatly simplify and the moments read:

$$\langle \xi_{fix}^q \rangle \simeq \frac{A_q + B_q}{1 + \eta/\bar{\gamma}_0} \quad (33)$$

i.e., they behave like $\langle \xi_{fix}^q \rangle \sim Y^q$. For the cumulant moments the leading terms cancel and

$$K_{q,fix} \sim Y. \quad (34)$$

This can be easily seen by noting that at high energies eq. (30) can be approximately written as

$$D(\omega, Y) \simeq \exp[\gamma_\omega Y] \quad \text{with} \quad \gamma_\omega = -\left(\frac{\omega}{2} + \eta\right) + \tilde{\omega} \quad (35)$$

Since the coupling in this case is frozen, the anomalous dimension γ_ω does not depend on y , the integral in eq. (24) becomes trivial and eq. (34) follows directly.

3 Moment analysis

3.1 Determination of moments and mass effects

In order to determine the moments one has to integrate the ξ -spectra over the full range. Here one faces a problem for small momenta because of mass effects as already discussed in [18]. In the theoretical calculation the partons are treated as massless with $k_{\perp} > Q_0$, therefore $\xi \equiv \xi_E = \ln \frac{P}{E} \leq Y = \ln \frac{P}{Q_0}$, i.e. ξ has an upper limit. On the other hand, the experimental data usually refer to the distribution in particle momentum p or $\xi_p = \ln \frac{P}{p}$, and ξ_p is not limited from above.

For identified particles with known masses one can easily construct the energy distributions, but there is no reliable prediction yet for the mass dependence of the identified particle spectra within the theoretical framework considered here. Therefore we restrict ourselves to charged particles and we give them a common effective mass m_h . If this mass is taken equal to the cut-off Q_0 , then for partons and charged particles there is the same upper limit $\xi_E = Y$. The hadron spectra in the jet from the primary parton A are then calculated from the parton distribution according to the LPHD hypothesis from [22,18]

$$E_h \frac{dn_A(\xi_E)}{dp_h} = K_h E_p \frac{dn_A(\xi_E)}{dp_p} \equiv K_h D_A^g(\xi_E, Y) \quad (36)$$

with $E_h = \sqrt{p_h^2 + Q_0^2}$ and K_h an unknown normalization constant to be fitted by the data. Eq. (36) leads to the correct relation for $p \sim E \gg Q_0$, independent of the mass; for small momenta it yields a finite value for the invariant density $E \frac{dn}{d^3p}$ in agreement with the data [18] (see also the discussion on this point in [23]). As Q_0 has the meaning of a transverse momentum cut-off for partons, it could be thought of for hadrons as an effective transverse mass $m_T = \sqrt{m^2 + p_{\perp}^2}$, which is larger than the particle mass itself.

The effect of introducing an effective particle mass on the shape of the spectrum is shown in Fig. (1). Here the inclusive charged particle ξ -spectra with different mass assignments, namely $Q_0 = 0$, $Q_0 = m_{\pi}$ and $Q_0 = 270$ MeV, are shown. The latter value is suggested from the moment analysis [18], see below. The upper limits of ξ corresponding to the above effective masses Q_0 are also shown in the figures. As can be seen from these figures, the rescaling procedure is relevant in the soft region only, where the kinematical boundary becomes important. The effect is stronger at the lower \sqrt{s} energy of $\sqrt{s} = 14$ GeV [10] as compared to $\sqrt{s} = 91$ GeV [11]. In the latter case the separation of curves in the measured range is hardly visible.

The moments $\langle \xi^q \rangle$ are determined from the spectra $E dn/dp$ vs. ξ_E after appropriate transformation of the measured x_p spectra and therefore

depend on the chosen effective mass $m_h = Q_0$. For the unmeasured interval near $\xi_E \simeq Y$ (small momenta), we added an extra-point with coordinates $\{(Y + \xi_{last})/2, D(\xi_{last})/2 \pm \sigma_D(\xi_{last})\}$ to linearly interpolate between the last measured point of coordinates $\{\xi_{last}, D(\xi_{last}) \pm \sigma_D(\xi_{last})\}$ and the limit $\{Y, 0\}$ imposed by kinematics. The errors of the moments are determined from the errors of $D(\xi_i)$ and the errors of the central values of ξ_E in each bin, taken as half the bin-size.

Correspondingly, we obtain the multiplicity $\overline{\mathcal{N}}_E$ as integral over ξ_E of the full spectrum $E dn/dp$. As expected from Fig. (1), its difference to the usual particle multiplicity $\overline{\mathcal{N}}_{ch}$ decreases with rising cms energy, from 30% at $\sqrt{s} = 3$ GeV to 10% at LEP energy. The MARK I data point at $\sqrt{s} = 4.03$ GeV shows an anomalous decrease of up to 50%, which may be partly related to charm thresholds effects. The result of this moment determination using the effective mass $Q_0=270$ MeV is presented in Table 1; this value of Q_0 results from the fit discussed below.

3.2 QCD description of moments for running α_s

3.2.1 Determination of the parameters Q_0 and Λ

The study of cumulant moments of the charged particle energy spectra allows for the first time the unconstrained determination of the two essential parameters which enter the theoretical predictions, namely Q_0 and Λ (or λ) for the running α_s model and Q_0 and γ_0 for the fixed α_s model. Let us start with the running α_s case with results shown in Fig. (2), the analysis of the fixed α_s results, shown in Fig. (3), runs parallel and will be discussed below.

Fig. (2) shows the mean multiplicity, the average value $\bar{\xi}_E$ and the dispersion σ^2 extracted from the experimental data [10,11,12,13,14,24,25,26,27,28,29] as a function of the cms energy for three different values of the parameter Q_0 ; the theoretical predictions for the cumulant moments using the given Q_0 still depend on Λ (or λ). The predictions are calculated for the number of flavours $n_f = 3$. For the particle multiplicity we use

$$\overline{\mathcal{N}}_E = c_1 \frac{4}{9} 2\overline{\mathcal{N}}_{part} + c_2 \quad (37)$$

with arbitrary parameters c_i and parton multiplicity $\overline{\mathcal{N}}_{part}$ from eq. (29) (the factor 4/9 is for the quark jet and 2 is for the two hemispheres). The two normalization parameters are determined to let the curve go through the lowest and the highest energy data points. The parameter c_1 corresponds to the K_h factor in eq. (36), whereas the additional parameter c_2 has been introduced to allow for a finite multiplicity at threshold as in (25). It is

important to note that the higher moments ($q \geq 1$) describe the shape and do not depend on the normalization, so they are unaffected both by the systematic experimental uncertainties of the overall normalization and by the theoretical uncertainties associated with the K_h factor.

The mean multiplicity data in Fig. (2), for each chosen Q_0 , can be properly described by the theoretical predictions for any value of λ in the range $0 \leq \lambda \leq 4$. Let us stress that the theoretical predictions at parton level strongly depend on λ , but one can obtain in all cases good fits of the experimental data by adjusting the free parameters c_i in eq. (37). Therefore the mean multiplicity data alone do not determine the parameter λ . Looking now at the first moment $\bar{\xi}$, we observe that for each chosen Q_0 a suitable value of λ can be found which provides a good description of the data. In order to fix both parameters, one has then to include the dispersion σ^2 . As can be seen from the figure, a lowering of Q_0 shifts both the $\bar{\xi}_E$ and the σ^2 data downwards. On the other hand, an increase of λ yields lower values for $\bar{\xi}_E$ but larger values for σ^2 , as one can see by inspection of the first two terms in the expansion of $\bar{\xi}_E$ and σ^2 in λ [18].

The parameters Q_0 and λ are determined from a χ^2 -minimization. To compute the χ^2 we have used the first 4 moments ($q \geq 1$) of the inclusive energy spectra for charged particles, but not the mean multiplicity because of its larger systematic errors and the need of two more normalization parameters for its theoretical description. The minimum of χ^2 is obtained for the limiting spectrum ($\lambda \rightarrow 0$), and the parameters are estimated as:

$$Q_0 \simeq \Lambda \simeq 270 \text{ MeV.} \quad (38)$$

The minimum value of the $\chi^2/d.o.f.$, neglecting the correlations among the cumulants of different order, is found to be 1.8 (with about 70 *d.o.f.*). So we do not obtain a “perfect” fit of the data, but considering the small errors of the lowest order moments and the small number of parameters, a very satisfactory description of all moments over a large energy range is obtained. In view of the systematic uncertainties of the fit we estimate the errors of the parameters from the limiting case in which the theoretical curves miss all data points by about one standard deviation. This yields the conservative estimate

$$\Delta Q_0 \simeq \Delta \Lambda \simeq 20 \text{ MeV.} \quad (39)$$

Alternatively, this result can also be transformed into a limit on $\lambda = \ln(Q_0/\Lambda)$

$$\lambda \lesssim 0.1. \quad (40)$$

Our result (38) is slightly larger than the ~ 250 MeV obtained by the OPAL Collaboration[11] from a fit of the measured ξ distribution to the limiting

spectrum adjusting only one parameter. The small difference results from the inclusion of lower energy data in our fit.

3.2.2 Discussion of the fits

The cumulant moments up to order $q = 4$ together with the corresponding predictions for the limiting spectrum with $Q_0 = 270$ MeV and $n_f = 3$ are shown in Fig. (4) by the solid lines. The values of the moments and the corresponding theoretical predictions are given also in Table 1. A very satisfactory description is obtained in the full *cms* energy range available; small deviations in the first moment at very low energies are visible. This may signal some limitations of the approximations involved, in particular, the simplified relation between quark- and gluon-jets, in this region.

It should be noted that the moments with $q \geq 1$ are determined by two parameters only which actually almost coincide. This should be contrasted with the more conventional applications of perturbative QCD to the particle or parton spectra. There one starts at a finite energy Y_0 with a non-perturbative input distribution which in general requires a set of unknown parameters and then evolves this distribution to higher energies according to the predictions of perturbative QCD. In terms of moments this would require one adjustable value $K_q(Y_0)$ for each moment at the initial energy Y_0 .

In the application of LPHD one assumes the validity of the perturbative formulae for the moments down to small energy scales of order few hundred MeV, actually down to the threshold energy Q_0 , where the distribution function is known to be simply the δ -function (10). In this limit all the higher moments are determined to be zero. Therefore the compact description with only two parameters is a direct consequence of the assumption that the theoretical description can be continued down to these low energies. A free adjustment of the moments at higher energy Y_0 with a vertical shift of the curves in Fig. (4) would not improve the predictions essentially; the limiting spectrum with the absolute normalization at threshold gives indeed the best results. It should be noted that the previous applications of the limiting spectrum to fit the ξ -spectra (for example [3,11]) rely on the same assumption that the QCD evolution can be continued down to the low scales Q_0 of few hundreds MeV where the initial condition is introduced.

3.2.3 Flavour dependence

The theoretical predictions shown so far were obtained with 3 active flavours. A possible source of uncertainty in the theoretical formulae is the number of active flavours to be used (see also [18,15]). In the predictions for cumulants

(24) the number of flavours enters essentially through the running coupling $\alpha_s(y, n_f)$. We neglect in the present discussion the additional explicit dependence at the percent level, which comes in through the parameter a at the next-to-leading order of the MLLA.

The moments evolve at low energy with 3 active flavours and with 4 and 5 flavours after passing the respective thresholds. The simplest approach would be to put the thresholds at the heavy quark masses, i.e., to increase n_f by one at $\frac{\sqrt{s}}{2} = m_Q$ where $\sqrt{s} = 2P$. However, let us recall that the argument of α_s is the transverse momentum k_\perp and kinematics forces $k_\perp \leq \frac{1}{4}\frac{\sqrt{s}}{2}$. This suggests moving the thresholds to $\frac{\sqrt{s}}{2} = 4m_Q$ (or towards even larger values, see for example [30]).

In Fig. (4) we show the predictions from the limiting spectrum with the inclusion of heavy flavours at the corresponding thresholds $\frac{\sqrt{s}}{2} = 4m_Q$ (dashed lines). Above a heavy quark threshold the moments evolve according to (24) with the respective number of active flavours n_f and match continuously to the moments with $n_f - 1$ active flavours below the threshold, in complete analogy to the inverse coupling constant $1/\alpha_s$ [31]. We then write for the cumulants

$$K_q\left(\frac{\sqrt{s}}{2}\right) = K_q^{(n_f)}\left(\frac{\sqrt{s}}{2}\right) - \sum_{i=4}^{n_f} \left(K_q^{(i)}(4m_f) - K_q^{(i-1)}(4m_f) \right) \Theta\left(\frac{\sqrt{s}}{2} - 4m_f\right) \quad (41)$$

Here $K_q^{(i)}(P_{jet})$ refers to the moment calculated with i flavours from threshold Q_0 up to jet momentum P_{jet} . The comparison of the upper two curves in Fig. (4) shows that the inclusion of the heavy quark thresholds does not modify dramatically the behaviour of the moments. Therefore, a reasonable approximation of the experimental data in the present energy range is obtained by taking into account only three active flavours throughout the full energy range. This behaviour of the theoretical predictions can be easily understood from the representation of the moments (24) in terms of the anomalous dimension. Just above threshold the contribution of the new flavour to the y -integral is negligible. Most primary gluons are still emitted at a smaller scale below the new flavour threshold. On the other hand, an approximation with five flavours in the full energy range would be a complete failure.

We have neglected here the differences in the light and heavy quark fragmentation. Whereas such effects occur in the fragmentation region, they are expected to be small in our application, as the soft gluon radiation is universal.

3.2.4 The effect of a light gluino

By exploiting the flavour dependence one can also extract new information on the possible presence of additional light particles. There has been considerable interest in the last years in the question whether there is a supersymmetric gluino with a small mass. In a recent summary [32] the gluinos in the mass range $1\frac{1}{2}$ – $3\frac{1}{2}$ GeV are considered as absolutely excluded, whereas lighter gluinos are allowed, except for certain ranges of lifetime. In a recent study [33] of jet rates and jet angular distributions in the reaction $e^+e^- \rightarrow 4$ jets, such a possibility has been severely restricted, however.

A sensitive probe of the presence of light gluinos is the running of α_s [34], as each gluino changes the number of active flavours by 3. Here we show the sensitivity of the moments to the presence of a light gluino with mass around 1 GeV. It is assumed that the effect of the light gluino comes in only through the running coupling and not through its effect on the final state structure. This can be justified by noting that gluino pair production – like quark pair production – does not contribute to the cascade evolution in leading double log order. In Fig. (4) the lowest curve represents the predictions for the moments assuming the presence of one light gluino with 1 GeV mass, i.e., 3 additional flavours at $\frac{\sqrt{s}}{2} \geq 4$ GeV.

The multiplicity $\overline{\mathcal{N}}$ can be fitted again by readjusting the normalization parameters in agreement with previous findings [35]. On the other hand, the predictions for the higher moments, especially with $q = 2$ and $q = 3$, are far off the data. The energy dependence of the moments in presence of the light gluino is weaker in the same way as the running of α_s is weaker, as it is expected from eq. (24). We conclude that the existence of a light gluino is not supported by our analysis. However, it seems premature to definitely exclude such a particle at present from this study. There are some simplifications in the present analysis and our QCD fit without gluino is not perfect in a χ^2 sense. Since the moments are very sensitive to the existence of a light gluino, a meaningful statistical test could be performed after a further improvement of the theoretical description.

3.3 Results for fixed α_s

To see the effect of the running coupling in the inclusive energy spectra, let us now consider for comparison the corresponding model with fixed coupling. Fig. (3) contains the same data as Fig. (2), but the theoretical predictions refer now to the MLLA with fixed α_s [18]. The curves correspond to three different values of the coupling α_s , i.e., of the anomalous dimension γ_0 . For the multiplicity we take eq. (37) with $\overline{\mathcal{N}}_{part}$ given by eq. (31). Again, the

parameter γ_0 cannot be extracted from the study of the mean multiplicity alone. Including the other two cumulants, one can reproduce at best, choosing $\gamma_0 = 0.64$ (i.e., $\alpha_s = 0.21$), the multiplicity data and the energy slope of the first moment ξ_E , though not its absolute value.

In Fig. (5) we show the predictions of the fixed- α_s model with $\gamma_0 = 0.64$ (dashed lines), where the absolute normalization is determined again at threshold as in the case of the running coupling, see (32). We also investigated whether the agreement with data can be improved if the normalization at threshold is abandoned and shifted to a higher energy. To this end we introduced an additional parameter for each cumulant, which allows for vertical shifts of the curves; they have been chosen to fit the experimental points at $\sqrt{s} = 44$ GeV. In the following we will refer to this model as the shifted fixed- α_s model.

Contrary to the case of running α_s , the vertical shifts can improve the description of the moments for the model with fixed coupling, but only in a limited range of *cms* energies. Especially, the moments with $q \geq 3$ show a rather different trend with energy in comparison with the data.

In an alternative investigation of the relevance of the running coupling for the inclusive energy spectra, it has been proposed to look at the predictions of Monte Carlo programs with and without running coupling [36]. It was found that the JETSET Monte Carlo [37] with the standard hadronization phase but the coupling frozen at the value of $\alpha_s = 0.2$ in the perturbative phase describes the experimental data reasonably well throughout the PETRA/PEP energy range and deviations occur only at higher energies. At first sight this result seems to contradict our findings. Note, however, that in the JETSET Monte Carlo the perturbative evolution stops at a cut-off value of about 1 GeV, when the string fragmentation takes over. In our perturbative approach, we allow on the contrary the perturbative cascade to evolve down to the much smaller cut-off $Q_0 \sim 270$ MeV. It is in this low energy domain that the variation of the coupling is most pronounced. The running coupling becomes large especially for small k_\perp so that particles tend to be produced collimated. The perturbative calculations at low scales with running coupling seem to simulate the production and decay of resonances implemented in Monte Carlo programs like JETSET. This supports the idea that the parton cascade with running coupling down to small scales is dual to the cascade with a shorter perturbative phase but with hadronic resonances in the last stage [18].

3.4 Rescaled cumulants

In addition to the standard moment analysis performed in the previous subsection, let us also consider the rescaled cumulants $K_q/\bar{\xi}$. These quantities become energy independent in case of fixed coupling at high energies as follows directly from (34). In particular for the first three rescaled cumulants, one has

$$\frac{K_2}{\bar{\xi}} \simeq \frac{\gamma_0^2}{2\bar{\gamma}_0^2} \frac{1}{\eta + \bar{\gamma}_0} \quad , \quad \frac{K_3}{\bar{\xi}} \simeq -3 \frac{\gamma_0^2}{4\bar{\gamma}_0^4} \frac{\eta}{\eta + \bar{\gamma}_0} \quad , \quad \frac{K_4}{\bar{\xi}} \simeq \frac{3\gamma_0^2}{8\bar{\gamma}_0^6} \frac{4\eta^2 - \gamma_0^2}{\eta + \bar{\gamma}_0} \quad (42)$$

Therefore these ratios exhibit more directly the differences to the case of running coupling. In Fig. (6) the experimental data on these ratios, as derived from our moment results in Table 1, are compared to the MLLA predictions with running α_s , then with the fixed α_s and the shifted fixed- α_s models. Once again, a good description of data is given by the MLLA model with running coupling. The fixed- α_s model shows the expected behaviour, i.e., the rescaled cumulants tend to a constant value at large cms energies; its predictions lie far away from the experimental data. The odd moments, which vanish in the DLA, approach their asymptotic limits more slowly. In the shifted fixed- α_s model previously described, the behaviour of the rescaled cumulants changes and the predictions become closer to the data. However, the deviations from the running α_s predictions become obvious for the smaller and also the very high energies with $Y > 6$, where the ratios reflect the different asymptotic trends. For example, the ratio $K_4/\bar{\xi}$ changes curvature when going from fixed to running α_s . Data at these higher energies are becoming now available at the TEVATRON[16] and could give new information.

4 Analysis of the shape

4.1 Energy evolution of the shape

The moment analysis has selected the solution with similar values for the parameters Q_0 and Λ ; let us now consider the predictions for the shape of the spectrum itself. Fig. (7) shows the inclusive energy spectra Edn/dp as a function of ξ_E , extracted from experimental data [24,26,10,11,12] using the fitted cut-off parameter $Q_0 = 270$ MeV as the effective mass in the calculation of the particle energy. The curves show the predictions of the limiting spectrum with the same value of the Q_0 parameter. The normalization has been fixed by choosing the integral of the spectrum to be equal to the average multiplicity according to the formula (37), the respective numbers are also

given in Table 1. The fit describes well the main features of the data in the wide range of cms energies $7 \leq \sqrt{s} \leq 140$ GeV, especially in the region with ξ_E smaller than the peak position.

Some deviations of the fitted curves from the data can be seen for larger ξ_E 's, i.e., for smaller particle energies. At low cms energies the curves fall somewhat above the data near the peak position and below the data near the kinematic limit ($\xi \rightarrow Y$). This behaviour may be related to the fact that the limiting spectrum approaches a constant value and not zero for $\xi \rightarrow Y$, as expected for the exact solution of the evolution equations (10) or (12).

A iterative approximate solution of the MLLA equations which is valid in the soft region and goes to zero for $\xi \rightarrow Y$ has been given in [23]:

$$D(\xi, Y, \lambda)_{MLLA} = D(\xi, Y, \lambda)|_{DLA} \exp \left[-a \int_{\xi}^Y \frac{\gamma_0^2(y)}{4N_C} dy \right] \quad (43)$$

where

$$D(\xi, Y, \lambda)|_{DLA} = \frac{4C_A}{b} \ln \left(1 + \frac{Y - \xi}{\lambda} \right) \left[1 + \frac{\frac{4N_C}{b} \int_0^{Y-\xi} d\tau \ln(1 + \frac{\tau}{\lambda}) \ln(1 + \frac{\xi}{\tau+\lambda})}{\ln(1 + \frac{Y-\xi}{\lambda})} \right] + \dots \quad (44)$$

In Fig. (8) the theoretical predictions from this approximation are compared with the same data as in Fig. (7) for low particle energies $E < 1$ GeV. A rather good description of data in the soft region is obtained in this way, in agreement with previous findings on the quantity Edn/d^3p [23].

4.2 High energy limit of the spectrum and ζ -scaling

In QCD the asymptotic behaviour of the soft production phenomena can be derived within the DLA, which takes into account the leading collinear and soft singularities originating from the Bremsstrahlung processes. A well known scaling law of this type is the KNO scaling [40,41,42] of the particle multiplicity distribution for rescaled probabilities and multiplicities.

Within QCD the momentum spectra do not scale asymptotically in the Bjorken or Feynman variables $x = p/P$ because of the Bremsstrahlung emissions with large transverse momenta, as is well known. Instead, they approach a finite scaling limit in certain rescaled logarithmic variables. This proposal, put forward already more than ten years ago [20], has never been studied since. A scaling behaviour of similar type for angular correlations has been recently proposed [43] and found some support by experimental data [44].

The asymptotic behaviour of the inclusive energy spectrum can be derived from the DLA evolution equation, i.e. (12) with $a = 0$. One finds a scaling law in the rescaled logarithmic variable ζ for the rescaled spectrum [20]

$$\frac{\ln D(\xi, Y)}{\ln \overline{\mathcal{N}}(Y)} = F(\zeta) \quad , \quad \zeta = \frac{\xi}{Y} \quad (45)$$

independent of Y . The logarithmic variables naturally occur in the asymptotic limit as they absorb the Bremsstrahlung singularities in the evolution equation (6).

The scaling function $F(\zeta)$ takes in DLA the following form [20]:

$$F(\zeta) = \frac{\mu}{\sinh \mu} \quad \text{with} \quad 2\zeta - 1 = \frac{\sinh 2\mu - 2\mu}{2 \sinh^2 \mu} \quad (46)$$

The function $F(\zeta)$ is symmetric around $\zeta = 1/2$, where it has a maximum of 1, and it goes as $\sqrt{\zeta \ln 1/\zeta}$ for $\zeta \rightarrow 0$. In the MLLA model with fixed coupling explicit analytical expressions for the spectrum and for the average multiplicity are available[18] and the scaling function is given by $F(\zeta) = 2\sqrt{\zeta(1-\zeta)}$.

For further illustration of the scaling law (45), we recall the Gaussian approximation of the DLA [5,6]

$$D(\xi, Y) \simeq \frac{\overline{\mathcal{N}}(Y)}{((Y + \lambda)^{3/2} - \lambda^{3/2})^{1/2}} \exp\left(-\frac{3\sqrt{\frac{4N_C}{b}}(\xi - \frac{Y}{2})^2}{(Y + \lambda)^{3/2} - \lambda^{3/2}}\right) \quad (47)$$

As the multiplicity $\overline{\mathcal{N}}(Y) \sim \exp(\sqrt{16N_C(Y + \lambda)/b})$ at high energies, one finds in exponential accuracy

$$F(\zeta) \simeq 1 - \frac{3}{2}\left(\zeta - \frac{1}{2}\right)^2 \quad (48)$$

which depends only on ζ and not on Y . In case of fixed α_s the Gaussian is slightly narrower $F(\zeta) \simeq 1 - 2(\zeta - \frac{1}{2})^2$. The DLA asymptotic scaling functions both for running and fixed α_s and their Gaussian approximations are shown in Fig. (9). We notice that the two asymptotic curves for running and fixed α_s do not differ very much quantitatively in the region around the maximum $\zeta \sim 1/2$, but they do in the soft region, where the effect of the running of α_s becomes relevant [23] and the corresponding curve shows indeed a steeper slope than the fixed- α_s one. Notice also that the Gaussian approximation considerably deteriorates towards the limits $\zeta \sim 0$ and $\zeta \sim 1$.

It should be noted that only the transformed observable (45) and not the spectrum $D(\zeta, Y)$ itself approaches a finite limit. The spectrum $D(\zeta, Y)$ can

be approximated by a Gaussian in ζ with width $\sigma_\zeta^2 \sim 1/\sqrt{Y}$ and therefore one finds asymptotically for D and its moments

$$D(\zeta, Y) \rightarrow \delta(\zeta - \frac{1}{2}) \quad , \quad \langle \zeta^q \rangle \rightarrow \frac{1}{2^q} \quad (49)$$

The MLLA results for the moments (63)–(66) indeed approach this limit.

In Fig. (10) we show the experimental data for the observable (45) at three different *cms* energies [10,26,14]. In this figure ξ is chosen to be ξ_p and $Y = \ln(\sqrt{s}/2Q_0)$ with $Q_0 = 270$ MeV. Experimental data for the average charged multiplicity have been taken from [45,46,14]. Fig. (11) shows the same observable, but this time as a function of $\xi = \xi_E$, where the energy is calculated with the effective mass $Q_0 = 270$ MeV. In this way, experimental spectra have a common kinematical boundary at $\zeta_E = 1$ and can be compared with the theoretical predictions as in Fig. (7). Fig. (11) also shows the theoretical predictions of the Limiting Spectrum normalized by the average multiplicity (37) and (29) at the same *cms* energies of the experimental data, as well as the asymptotic DLA prediction of eq. (46).

One can see from these figures that the original energy evolution of the spectrum visible in Fig. (7) is largely removed if the scaling variables (45) are used. Some scaling violation remains, especially in the small ζ region. The limiting spectrum reproduces well the small scaling violations shown by the data. It approaches the asymptotic limit very slowly and only at unphysically large energies². The data at the present *cms* energies lie far away from the asymptotic DLA curve in the small ζ domain; however, it is interesting to notice that the data for soft particles ($p \sim 0$, $\xi \sim Y$, $\zeta \sim 1$) are already close to the asymptotic limit. This result lends further support to the idea that very soft particles are basically determined by the nearby Bremsstrahlung singularities and not affected by the non singular terms in the splitting functions taken into account in MLLA nor by the recoil effects (see [23] for a previous discussion of this point).

The energy dependence of the position of the maximum of the ζ distribution, ζ^* , is shown in Fig. (12) up to LEP-1.5 energies. Also in this case, the data closely follow the prediction of the limiting spectrum, which very slowly approaches the asymptotic DLA limit $\zeta^* = \frac{1}{2}$.

One concludes that the data show an approximate scaling law in the presently available energy range. However, this scaling is preasymptotic, i.e., the asymptotic shape of the distribution is quite different from the one observed at present energies. Similar results on the existence of a large

²For instance the scaling function $F(\zeta)$ at $\zeta = 1/2$, whose asymptotic value is 1, reaches 0.8 at $Y \sim 68$ ($\sqrt{s} \sim 10^{28}$ GeV) and 0.9 at $Y \sim 460$ ($\sqrt{s} \sim 10^{200}$ GeV).

preasymptotic scaling regime have also been predicted for the multiplicity scaling (KNO) and its violation [47,48]; in this case significant deviations from scaling are expected only around $\sqrt{s} \sim 1$ TeV [49].

5 Conclusions

The perturbative QCD approach has been shown to describe well experimental data on charged particle inclusive energy spectra in e^+e^- annihilation. The new features of the moment analysis of the spectrum have been discussed.

The first determination of the two independent essential parameters of the theory has been performed, whereby the best description of the data is obtained for $Q_0 \simeq \Lambda \simeq 270$ MeV with an uncertainty of about 20 MeV. The dependence of the moments on the initial conditions has been studied; if one takes the nonperturbative initial condition of the perturbative QCD evolution at the threshold of the process, a good description of the moments also in their absolute normalization is obtained in the full energy range available including the low energies of a few GeV. The sensitivity of the moments to the running of the coupling has been established by comparing the predictions of the full model with the predictions of a model with frozen coupling. The effect of heavy quark thresholds in the running of the coupling has also been discussed; a good phenomenological description of the data at present energies is obtained already by including only three active flavours. The moments are very sensitive to the presence of a light gluino with mass around 1 GeV, but there is no evidence for the type of effect expected.

The inclusive energy spectra themselves have also been studied. The limiting spectrum with $Q_0 = \Lambda$ is found to provide a good overall description of the data in a large cms energy range. An improvement in the soft region can be obtained by applying an approximation which takes into account the boundary conditions at $\xi = Y$ explicitly.

Data in the presently available cms energy range support an approximate scaling law, the ζ -scaling, predicted at asymptotic energies. Some violations of the scaling behaviour in this preasymptotic energy range are observed, as expected from the MLLA. The data in the soft energy region ($\zeta \lesssim 1$) at available energies are already close to the asymptotic predictions.

There are some simplifications both in the phenomenological analysis (for example, neglect of difference in light and heavy quark fragmentation) and the theoretical description. The respective improvements would yield a more stringent test of the theoretical scheme and possibly a quantitative improvement of the fit to the data. As the main result of the present analysis

we consider the good description of the data down to low scales – even if not entirely quantitatively everywhere – in agreement with QCD with running α_s and the LPHD picture.

References

- [1] A. Bassetto, M. Ciafaloni, G. Marchesini, Phys. Rep. **100** (1983) 202.
- [2] Yu. L. Dokshitzer, V.A. Khoze, A.H. Mueller, S.I. Troyan, Rev. Mod. Phys. **60** (1988) 373; “*Basics of Perturbative QCD*”, Editions Frontières, Gif-sur-Yvette CEDEX-France (1991).
- [3] Ya. I. Azimov, Yu. L. Dokshitzer, V. A. Khoze, S. I. Troyan, Z. Phys. **C27** (1985) 65; Z. Phys. **C31** (1986) 213.
- [4] V. A. Khoze and W. Ochs, “Perturbative QCD approach to multiparticle production”, preprint Durham DTP/96/36, MPI-PhT-96/29 (1996), to appear in Int. J. Mod Phys. A.
- [5] Yu. L. Dokshitzer, V. S. Fadin, V. A. Khoze, Phys. Lett. **B115** (1982) 242; Z. Phys. **C15** (1982) 325.
- [6] A. Bassetto, M. Ciafaloni, G. Marchesini and A. H. Mueller, Nucl. Phys. **B207** (1982) 189.
- [7] C. P. Fong and B. R. Webber, Nucl. Phys. **B355** (1991) 54.
- [8] B. I. Ermolaev and V. S. Fadin, JETP Lett. **33** (1981) 285.
- [9] A. H. Mueller, Phys. Lett. **B104** (1981) 161.
- [10] TASSO Coll., W. Braunschweig et al., Z. Phys. **C47** (1990) 187.
- [11] OPAL Coll., M. Z. Akrawy et al., Phys. Lett. **B247** (1990) 617.
- [12] ALEPH Coll., D. Buskulic et al., Z. Phys. **C73** (1997) 409.
- [13] DELPHI Coll., P. Abreu et al., Phys. Lett. **B372** (1996) 172.
- [14] OPAL Coll., G. Alexander et al., Z. Phys. **C72** (1996) 191.
- [15] V. A. Khoze, S. Lupia and W. Ochs, Phys. Lett. **B386** (1996) 451.
- [16] CDF Coll., A. Korytov, in Proc. of QCD '96, (Montpellier, France, 1996), Eds. S. Narison, Nucl. Phys. B (Proc. Suppl.) **54A** (1997) 67.
- [17] Yu. L. Dokshitzer, V. A. Khoze and S. I. Troyan, Int. J. Mod. Phys. **A7** (1992) 1875.
- [18] S. Lupia and W. Ochs, Phys. Lett. **B365** (1996) 339.

- [19] S. Lupia, in Proc. of QCD '96, (Montpellier, France, 1996), Eds. S. Narison, Nucl. Phys. B (Proc. Suppl.) **54A** (1997) 55;
W. Ochs, in Proc. XXXVI Cracow School of Theor. Phys., (Zakopane, Poland, 1996), Acta Phys. Pol. **B27** (1996) 3505.
- [20] Yu. L. Dokshitzer, V. S. Fadin and V. A. Khoze, Z. Phys. **C18** (1983) 37.
- [21] Yu. L. Dokshitzer and M. Olsson, Nucl. Phys. **B396** (1993) 137.
- [22] Yu. L. Dokshitzer, V. S. Fadin and V. A. Khoze, Phys. Lett. **B115** (1982) 242.
- [23] V. A. Khoze, S. Lupia and W. Ochs, Phys. Lett. **B394** (1997) 179.
- [24] MARK I Coll., J. L. Siegrist et al., Phys. Rev. **D26** (1982) 969.
- [25] MARK II Coll., J. F. Patrick et al., Phys. Rev. Lett. **49** (1982) 1232.
- [26] TOPAZ Coll., R. Itoh et al., Phys. Lett. **B345** (1995) 335.
- [27] ALEPH Coll., D. Buskulic et al., Z. Phys. **C55** (1992) 209.
- [28] DELPHI Coll., P. Abreu et al., Phys. Lett. **B347** (1995) 447.
- [29] L3 Coll., B. Adeva et al., Phys. Lett. **B259** (1991) 199.
- [30] W. Marciano, Phys. Rev. **D29** (1983) 580;
Yu. L. Dokshitzer, D. V. Shirkov, Z. Phys. **C67** (1995) 449.
- [31] G. Altarelli, Phys. Rep. **81** (1982) 1.
- [32] G. Farrar, Phys. Rev. **D51** (1995) 3904.
- [33] ALEPH Coll., R. Barate et al., CERN-PPE/97-002, January 97, subm. to Z. Phys. C.
- [34] I. Antoniadis, J. Ellis and D. V. Nanopoulos, Phys. Lett. **B262** (1991) 109.
- [35] F. Cuyppers, Z. Phys. **C61** (1994) 607.
- [36] F. Botterweck, private communication.
- [37] T. Sjöstrand, Computer Physics Commun. **82** (1994) 74.
- [38] H1 Coll., S. Aid et al., Nucl. Phys. **B445** (1995) 3.

- [39] ZEUS Coll., M. Derrick et al., *Z. Phys.* **C67** (1995) 93.
- [40] Z. Koba, H. B. Nielsen and P. Olesen, *Nucl. Phys.* **B40** (1972) 317.
- [41] A. M. Polyakov, *Sov. Phys. JETP* **32** (1971) 296; *ibid.* **33** (1971) 850.
- [42] A. Bassetto, M. Ciafaloni, G. Marchesini, *Nucl. Phys.* **B163** (1980) 477.
- [43] W. Ochs and J. Wosiek, *Phys. Lett.* **B304** (1992) 144; *Z. Phys.* **C68** (1995) 269.
- [44] DELPHI Coll., B. Buschbeck, F. Mandl et al., *Proc. XXIV Int. Symp. on Multiparticle Dynamics*, Sept. 1994, Vietri sul Mare, Salerno, Italy, Eds. A. Giovannini, S. Lupia and R. Ugoccioni, World Scientific, Singapore (1995) 52.
- [45] TASSO Coll., W. Braunschweig et al., *Z. Phys.* **C45** (1989) 193.
- [46] TOPAZ Coll., M. Yamauchi et al., *Proc. XXIV Int. Conf. on High Energy Physics* (Munich, 1988), Springer Verlag, Eds. R. Kotthaus and J. H. Kühn, p. 852.
- [47] E. D. Malaza, B. R. Webber, *Phys. Lett.* **B149** (1984) 501; *Nucl. Phys.* **B267** (1986) 70.
- [48] Yu. L. Dokshitzer, *Phys. Lett.* **B305** (1993) 295.
- [49] R. Ugoccioni, A. Giovannini and S. Lupia, *XXIV Int. Symp. on Multiparticle Dynamics 1994*, Vietri sul Mare, Italy, Sept. 1994, Eds. A. Giovannini et al., World Scientific, Singapore, p. 384 (1995).

A Explicit Formulae for Moments

A.1 Moments in the general case

The functions entering eq. (27) are defined as follows[17]: $\overline{\mathcal{N}} = \mathcal{N}_1 + \mathcal{N}_2$ is composed of two terms increasing and decreasing with energy, respectively,

$$\mathcal{N}_1 = \Gamma(B)\Gamma(1-B)z_1 \left(\frac{z_2}{z_1}\right)^B I_{B+1}(z_1)I_{-B}(z_2) \quad (50)$$

$$\mathcal{N}_2 = \Gamma(-B)\Gamma(B+1)z_1 \left(\frac{z_2}{z_1}\right)^B I_{-B-1}(z_1)I_B(z_2) \quad (51)$$

$$z_1 = \sqrt{16N_c(Y+\lambda)/b}; \quad z_2 = \sqrt{16N_c\lambda/b}.$$

The two terms build up the total multiplicity

$$\overline{\mathcal{N}} = z_1 \left(\frac{z_2}{z_1}\right)^B [I_{B+1}(z_1)K_B(z_2) + K_{B+1}(z)I_B(z_2)] \quad (52)$$

The functions $L_k^{(q)}$ and $R_k^{(q)}$ in (27) are computed from

$$L_k^{(q)} = D_{q-k}(B+1, B+2, z_1)D_k(-B, 1-B, z_2) \quad (53)$$

$$R_k^{(q)} = D_{q-k}(0, -B, z_1)D_k(0, B+1, z_2) \quad (54)$$

$$D_k(g, c, z) = P_0^{(q)}(g, c, z) + \frac{2}{z} \frac{I_c(z)}{I_{c-1}(z)} P_1^{(q)}(g, c, z)$$

where $P_i^{(q)}$ are the polynomials

$$P_0^{(q)}(g, c, z) = \sum_{k=0}^{q-1} \alpha_{q-k}^{(q)} \left(\frac{2}{z}\right)^{2k}, \quad P_1^{(q)}(g, c, z) = \sum_{k=0}^{q-1} \beta_{q-k}^{(q)} \left(\frac{2}{z}\right)^{2k}. \quad (55)$$

The coefficients of highest order are given by

$$\alpha_q^{(q)} = \frac{1}{2^q}, \quad \beta_q^{(q)} = \frac{q}{2^q} \left(B + \frac{q-1}{3}\right) \quad (56)$$

whereas in lower order they can be found by solving a $q \times q$ linear system of equations. For the first four moments one finds explicitly ($(a)_n \equiv \Gamma(a+n)/\Gamma(a) = a(a+1)\dots(a+n-1)$):

$$\begin{aligned} \beta_1^{(q)} &= \frac{\Phi_{1-c}^{(q)}}{1-c}, & \beta_2^{(q)} &= \frac{\Phi_{2-c}^{(q)}}{(c-2)_2} - \frac{\Phi_{1-c}^{(q)}}{(c-1)_2} \\ \beta_3^{(q)} &= -\frac{1}{2} \frac{\Phi_{3-c}^{(q)}}{(c-3)_3} + \frac{\Phi_{2-c}^{(q)}}{(c-2)_3} - \frac{1}{2} \frac{\Phi_{1-c}^{(q)}}{(c-1)_3} \end{aligned} \quad (57)$$

$$\begin{aligned}
\alpha_1^{(q)} &= \frac{\Phi_{1-c}^{(q)}}{(c-1)_2}, & \alpha_2^{(q)} &= -\frac{\Phi_{2-c}^{(q)}}{(c-2)_3} - \frac{\Phi_{1-c}^{(q)}}{(c-1)_3} \\
\alpha_3^{(q)} &= \frac{1}{2} \frac{\Phi_{3-c}^{(q)}}{(c-3)_4} - \frac{\Phi_{2-c}^{(q)}}{(c-2)_4} + \frac{1}{2} \frac{\Phi_{1-c}^{(q)}}{(c-1)_4}
\end{aligned} \tag{58}$$

in terms of the expressions

$$\Phi^{(1)} = \frac{1}{2}(n-1)_2 + gn \tag{59}$$

$$\Phi^{(2)} = \frac{1}{4}(n-2)_3 + (g + \frac{2}{3})(n-2)_3 + (g)_2(n-1)_2 \tag{60}$$

$$\begin{aligned}
\Phi^{(3)} &= \frac{1}{8}(n-5)_6 + (\frac{3}{4}g + 1)(n-4)_5 \\
&+ (\frac{3}{2}g^2 + \frac{7}{2}g + \frac{3}{2})(n-3)_4 + (g)_3(n-2)_3
\end{aligned} \tag{61}$$

$$\begin{aligned}
\Phi^{(4)} &= \frac{1}{16}(n-7)_8 + (\frac{1}{2}g + 1)(n-6)_7 + (\frac{3}{2}g^2 + \frac{11}{2}g + \frac{13}{3})(n-5)_6 \\
&+ (2g^3 + 10g^2 + 14g + \frac{24}{5})(n-4)_5 + (n-3)_4.
\end{aligned} \tag{62}$$

A.2 Limiting spectrum

In the special case $Q_0 = \Lambda$ we find [17] for the moments $q \leq 4$ explicitly:

$$\frac{\bar{\xi}}{Y} = \frac{1}{2} + \frac{B}{z} \frac{I_{B+2}(z)}{I_{B+1}(z)} \tag{63}$$

$$\frac{\langle \xi^2 \rangle}{Y^2} = \frac{1}{4} + \frac{B(B + \frac{1}{3})}{z^2} + \frac{(B + \frac{1}{3})}{z} \left(1 - \frac{2B(B + 2)}{z^2} \right) \frac{I_{B+2}(z)}{I_{B+1}(z)} \tag{64}$$

$$\begin{aligned}
\frac{\langle \xi^3 \rangle}{Y^3} &= \frac{1}{8} + \frac{3B(B + 1)}{2z^2} - \frac{2B^2(B + 1)(B + 3)}{z^4} + \\
&+ \frac{2}{z} \left[\frac{3B + 2}{8} - \frac{B(B + 1)(B + 3)}{z^2} + \frac{4B(B)_4}{z^4} \right] \frac{I_{B+2}(z)}{I_{B+1}(z)}
\end{aligned} \tag{65}$$

and

$$\begin{aligned} \frac{\langle \xi^4 \rangle}{Y^4} &= \frac{1}{16} + \alpha_3^{(4)} \left(\frac{2}{z}\right)^2 + \alpha_2^{(4)} \left(\frac{2}{z}\right)^4 + \alpha_1^{(4)} \left(\frac{2}{z}\right)^6 + \\ &+ \frac{2}{z} \left[\frac{B+1}{4} + \beta_3^{(4)} \left(\frac{2}{z}\right)^2 + \beta_2^{(4)} \left(\frac{2}{z}\right)^4 + \beta_1^{(4)} \left(\frac{2}{z}\right)^6 \right] \frac{I_{B+2}(z)}{I_{B+1}(z)} \end{aligned} \quad (66)$$

where

$$\alpha_3^{(4)} = 10 \frac{\Phi_{-B}^{(4)}}{(B)_5} - \frac{1}{4} \frac{B(B+1)(B+3)}{B-1} \quad (67)$$

$$\alpha_2^{(4)} = -3 \frac{\Phi_{-B}^{(4)}}{(B)_4} \quad , \quad \alpha_1^{(4)} = \frac{\Phi_{-B}^{(4)}}{(B+1)_2}$$

and

$$\beta_3^{(4)} = -6 \frac{\Phi_{-B}^{(4)}}{(B-1)_5} + \frac{1}{4} \frac{(B)_4}{B-1} \quad (68)$$

$$\beta_2^{(4)} = 2 \frac{\Phi_{-B}^{(4)}}{(B)_3} \quad , \quad \beta_1^{(4)} = -\frac{\Phi_{-B}^{(4)}}{(B+1)}$$

and

$$\begin{aligned} \Phi_{-B}^{(4)} &= \frac{1}{16} B^8 + \frac{3}{4} B^7 + 3.45833 B^6 + 7.7 B^5 \\ &+ 8.39583 B^4 + \frac{15}{4} B^3 + \frac{1}{12} B^2 - \frac{1}{5} B. \end{aligned} \quad (69)$$

A.3 Fixed coupling

The first coefficients A_q , B_q in (32) read (here $\rho \equiv \eta/\bar{\gamma}_0$)

$$A_1 = (\rho^2 + 1) \frac{Y}{2} \quad , \quad B_1 = (-\rho^2 - 1) \frac{1}{2\bar{\gamma}_0} + \rho Y ; \quad (70)$$

$$A_2 = (-3\rho^3 - \rho) \frac{Y}{4\bar{\gamma}_0} + (3\rho^2 + 1) \frac{Y^2}{4} \quad , \quad (71)$$

$$B_2 = (3\rho^3 + \rho) \frac{1}{4\bar{\gamma}_0^2} + (-3\rho^2 - 1) \frac{Y}{4\bar{\gamma}_0} + (\rho^3 + 3\rho) \frac{Y^2}{4} ;$$

$$A_3 = (15\rho^4 - 3)\frac{Y}{8\bar{\gamma}_0^2} - 12\rho^3\frac{Y^2}{8\bar{\gamma}_0} + (\rho^4 + 6\rho^2 + 1)\frac{Y^3}{8}, \quad (72)$$

$$B_3 = (-15\rho^4 + 3)\frac{1}{8\bar{\gamma}_0^3} + 12\rho^3\frac{Y}{8\bar{\gamma}_0^2} + (-6\rho^4 - 6\rho^2)\frac{Y^2}{8\bar{\gamma}_0} + (4\rho^3 + 4\rho)\frac{Y^3}{8};$$

$$A_4 = (-105\rho^5 + 30\rho^3 + 27\rho)\frac{Y}{16\bar{\gamma}_0^3} + (75\rho^4 - 18\rho^2 - 9)\frac{Y^2}{16\bar{\gamma}_0^2} \quad (73)$$

$$+ 2(-5\rho^5 - 14\rho^3 + 3\rho)\frac{Y^3}{16\bar{\gamma}_0} + (5\rho^4 + 10\rho^2 + 1)\frac{Y^4}{16},$$

$$B_4 = (105\rho^5 - 30\rho^3 - 27\rho)\frac{1}{16\bar{\gamma}_0^4} + (-75\rho^4 + 18\rho^2 + 9)\frac{Y}{16\bar{\gamma}_0^3}$$

$$+ (45\rho^5 + 18\rho^3 - 15\rho)\frac{Y^2}{16\bar{\gamma}_0^2} + 2(-15\rho^4 - 2\rho^2 + 1)\frac{Y^3}{16\bar{\gamma}_0}$$

$$+ (\rho^5 + 10\rho^3 + 5\rho)\frac{Y^4}{16}.$$

Table Caption

Tab. 1: The average multiplicity $\overline{\mathcal{N}}_E$, the average value $\bar{\xi}_E$, the dispersion σ^2 , the skewness s and the kurtosis k of charged particle inclusive energy spectra $E dn/dp$ vs. ξ_E for $Q_0 = 270$ MeV at various cms energies \sqrt{s} . In brackets theoretical predictions of the limiting spectrum of MLLA with running α_s ; the second entry in the average multiplicity column contains the results of eq. (37) with eq. (29); the first one the results with $c_2 = 0$. Errors on the average multiplicity data points include both statistical and systematic errors. Results at LEP and LEP-1.5 cms energies from [15].

Figure Captions

Fig. 1: **a)** Comparison of charged particle inclusive single particle spectra, Edn/dp vs. ξ , at $\sqrt{s} = 14$ GeV[10] for different mass assignment: the inclusive momentum spectrum pdn/dp vs. ξ_p (diamonds) and the rescaled spectra Edn/dp vs. ξ_E , with $E^2 = p^2 + Q_0^2$, $Q_0 = 138$ MeV (triangles) and $Q_0 = 270$ MeV (squares). Also shown are the upper limits of ξ_E given by $Y = \ln(\sqrt{s}/2Q_0)$; **b):** same as in **a)**, but at $\sqrt{s} = 91$ GeV[11].

Fig. 2: Dependence on Y of the three lowest order moments of the inclusive energy spectrum. The data of the mean multiplicity \overline{N}_E , average value ξ_E and dispersion σ^2 of inclusive energy spectra for $Q_0 = 138$ MeV (triangles), $Q_0 = 270$ MeV (diamonds) and $Q_0 = 350$ MeV (squares) are compared with theoretical predictions of MLLA with running coupling with $\lambda = 0$ (limiting spectrum) (solid line), $\lambda = 0.5$ (dashed line), $\lambda = 4$ (dotted line). The theoretical predictions for the mean multiplicity are computed from eqs. (37) and (29).

Fig. 3: Same data as in Fig. 2 for different Q_0 parameters; comparison with theoretical predictions of MLLA with fixed coupling with $\gamma_0 = 0.64$ (solid line), $\gamma_0 = 0.4$ (dashed line), $\gamma_0 = 1$ (dotted line). The theoretical predictions for the mean multiplicity are computed from eqs. (37) and (31).

Fig. 4: The average multiplicity \overline{N}_E and the first four cumulants of charged particle energy spectra Edn/dp vs. ξ_E , are shown as a function of $Y = \ln(\sqrt{s}/2Q_0)$ for $Q_0 = 270$ MeV at various cms energies (see Table 1). The curves show the predictions of the limiting spectrum with $Q_0 = 270$ MeV with 3 active flavours (solid line), the number of flavours n_f variable with the heavy quark thresholds at $\sqrt{s}/2 = 4m_Q$ (dashed line) and the inclusion of a light gluino with mass of 1 GeV (dotted line). In all cases, the mean multiplicity is computed from eqs. (37) and (29).

Fig. 5: Same data as in Fig. 4, but the curves show the predictions of the limiting spectrum (i.e. $Q_0 = \Lambda$) of MLLA with running α_s (solid line), of MLLA with fixed α_s (dashed line) and of the shifted fixed α_s model (dotted line); $n_f = 3$ everywhere.

Fig. 6: Rescaled cumulants $K_q/\overline{\xi}_E^q$ as a function of $Y = \ln(\sqrt{s}/2Q_0)$ for $Q_0 = 270$ MeV. Data as in Fig. 4 are compared with the corresponding predictions of the limiting spectrum of MLLA with running α_s (solid line). The dashed curve shows the predictions of the model with fixed α_s ($\gamma_0 = 0.64$); in this case, the rescaled cumulants approach constant values at high energies (0.534, 0.344, 0.528 respectively, with the chosen value of γ_0). Predictions of the shifted fixed α_s model are also shown (dotted line).

Fig. 7: Comparison of inclusive spectra Edn/dp vs. ξ_E , with $E^2 = p^2 + Q_0^2$, $Q_0 = 270$ MeV at various cms energies with predictions of the limiting spectrum (K_h fixed at each energy from the fit of eqs. (37) and (29)). Each curve is shifted up by 0.5 for clarity.

Fig. 8: Comparison of inclusive spectra Edn/dp vs. ξ_E , with $E^2 = p^2 + Q_0^2$, $Q_0 = 270$ MeV at various cms energies with predictions of the MLLA iterative solution (43) ($Q_0 = 270$ MeV, $\lambda = 0.01$, $K_h = 0.45$). Data and predictions for particle energies $E \leq 1$ GeV are shown.

Fig. 9: The DLA asymptotic prediction (46) for the scaling function $F(\zeta)$, the prediction of the Gaussian Approximation (48) and the corresponding predictions with fixed α_s in comparison.

Fig. 10: Test of ζ -scaling for the momentum spectra at 14, 58 and 130 GeV[10,26,14] with average charged multiplicities taken from [45,46,14].

Fig. 11: Test of ζ -scaling for the energy spectra. Data as in Fig. 10, but the particle energy is calculated using the mass $Q_0 = 270$ MeV, in comparison with theoretical predictions from the limiting spectrum ($Q_0 = 270$ MeV) normalized to the predicted average multiplicity according to eqs. (37) and (29). The DLA prediction (46) at asymptotic cms energy is also shown.

Fig. 12: Maximum of the rescaled inclusive momentum distribution $\zeta^* = \xi^*/Y$ as a function of $Y = \ln \frac{\sqrt{s}}{2Q_0}$; comparison between experimental data at various cms energies[10,11,12,13,14,24,25,26,27,28,29] and theoretical prediction in MLLA, numerically extracted from the shape of the limiting spectrum (solid line) for the cut-off parameter $Q_0 = \Lambda = 270$ MeV [15]. Crosses mark the predictions at the cms energies 200 GeV and 500 GeV. The asymptotical DLA result $\zeta^* = \frac{1}{2}$ is also shown (dashed line).

Table 1

Exp. \sqrt{s} (GeV)	$\bar{\mathcal{N}}_E$	$\bar{\xi}_E$	σ^2	s	k
MARK I[24]	3.01±0.3	1.02±0.02	0.14±0.01	-0.50±0.17	-0.46±0.13
3.0	(2.10,input)	(1.14)	(0.13)	(-0.50)	(-0.50)
MARK I[24]	3.66±0.37	1.27±0.02	0.17±0.01	-0.58±0.08	-0.12±0.20
4.03	(2.73,3.61)	(1.33)	(0.18)	(-0.48)	(-0.51)
MARK II[25]	±	1.47±0.04	0.19±0.01	-0.57±0.08	-0.20±0.17
5.2	(3.36,4.21)	(1.49)	(0.22)	(-0.47)	(-0.52)
MARK I[24]	4.63±0.46	1.61±0.03	0.26±0.01	-0.56±0.08	-0.29±0.18
7.4	(4.11,4.92)	(1.66)	(0.28)	(-0.45)	(-0.52)
TASSO[10]	7.64±0.59	2.10±0.04	0.40±0.01	-0.47±0.07	-0.42±0.17
14.	(6.73,7.40)	(2.12)	(0.44)	(-0.42)	(-0.52)
TASSO[10]	9.65±0.68	2.38±0.04	0.54±0.02	-0.47±0.07	-0.44±0.18
22.	(8.87,9.44)	(2.40)	(0.56)	(-0.40)	(-0.52)
TASSO[10]	12.21±0.86	2.67±0.03	0.68±0.01	-0.44±0.03	-0.51±0.09
35.	(11.51,11.95)	(2.69)	(0.70)	(-0.38)	(-0.52)
TASSO[10]	13.38±1.05	2.80±0.03	0.75±0.01	-0.40±0.04	-0.59±0.09
44.	(12.96,13.33)	(2.82)	(0.76)	(-0.37)	(-0.52)
TOPAZ[26]	14.54±0.43	3.01±0.03	0.80±0.02	-0.43±0.05	-0.49±0.15
58.	(15.09,15.34)	(3.00)	(0.85)	(-0.36)	(-0.52)
ALEPH[27]	18.81±1.05	3.24±0.04	0.99±0.05	-0.39±0.10	-0.59±0.32
DELPHI[28]	19.17±1.00	3.32±0.02	1.03±0.01	-0.40±0.02	-0.59±0.07
L3[29]	18.74±1.09	3.28±0.06	0.99±0.06	-0.35±0.13	-0.65±0.40
OPAL[11]	18.95±1.00	3.29±0.01	0.99±0.01	-0.36±0.03	-0.59±0.09
LEP-1 (avg)	18.93±0.52	3.29±0.01	1.01±0.02	-0.39±0.02	-0.59±0.05
DELPHI- γ [13]	19.20±0.26	3.33±0.04	0.99±0.03	-0.46±0.05	-0.44±0.18
91.2	(input,input)	(3.27)	(1.00)	(-0.35)	(-0.52)
ALEPH [12]	22.04±0.47	3.52±0.06	1.19±0.04	-0.37±0.07	-0.62±0.26
DELPHI [13]	22.27±0.58	3.47±0.05	1.13±0.05	-0.40±0.08	-0.49±0.29
OPAL [14]	21.50±0.57	3.51±0.07	1.19±0.04	-0.35±0.07	-0.63±0.25
LEP-1.5 (avg)	21.95±0.31	3.495±0.034	1.185±0.025	-0.365±0.042	-0.59±0.15
133	(22.6,22.5)	(3.50)	(1.14)	(-0.34)	(-0.52)

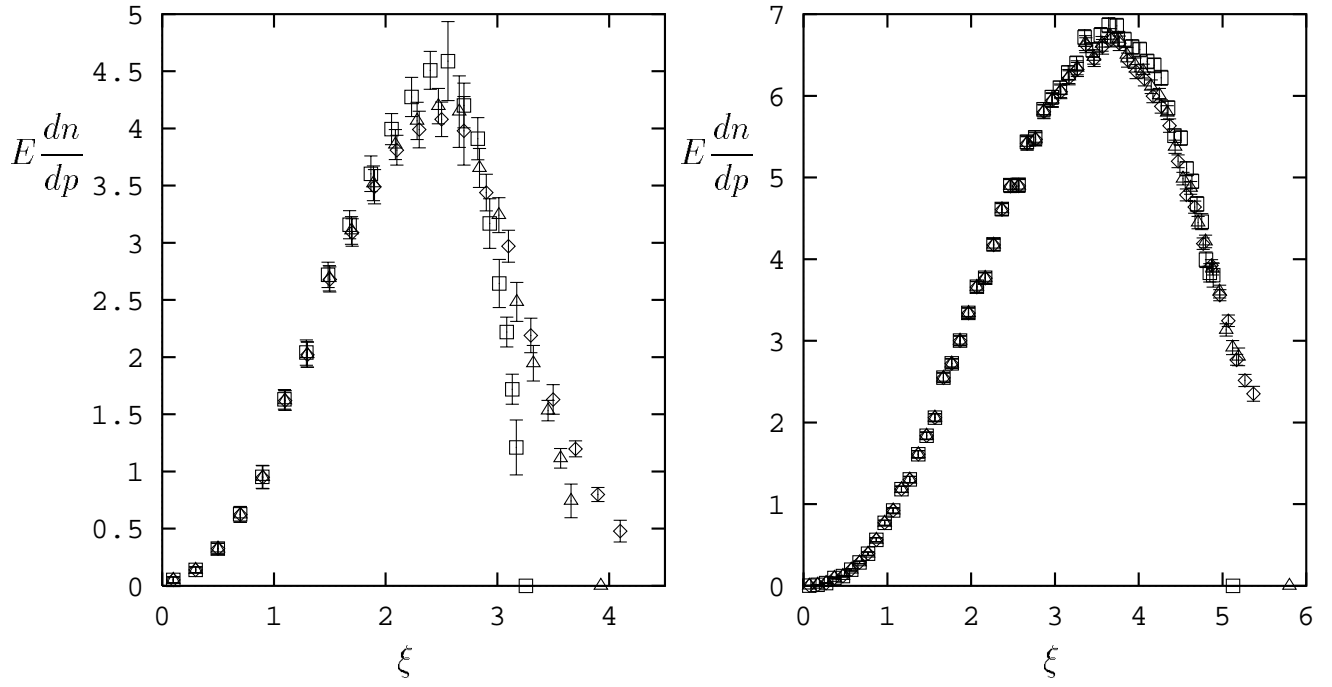


Figure 1:

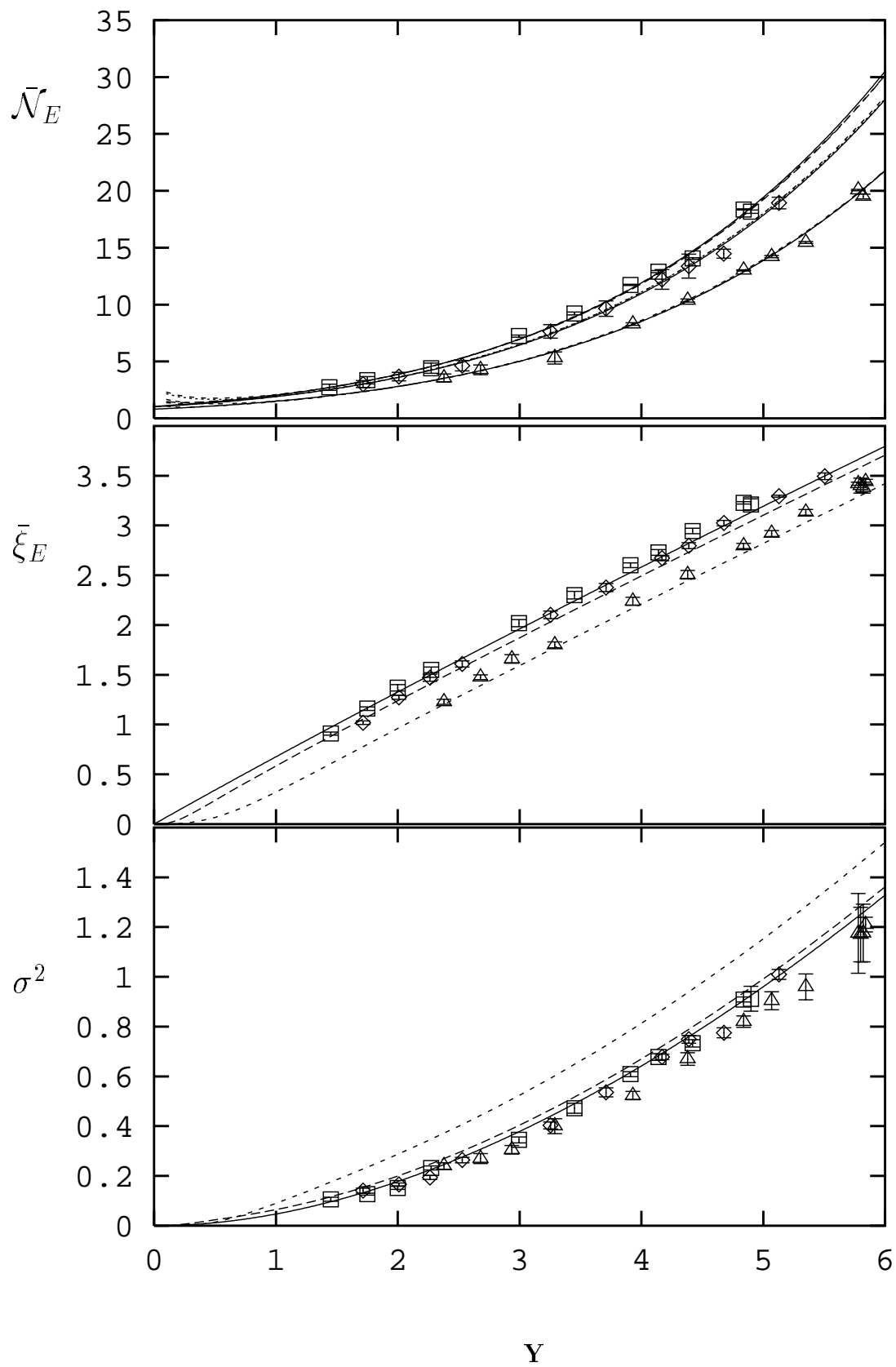


Figure 2:

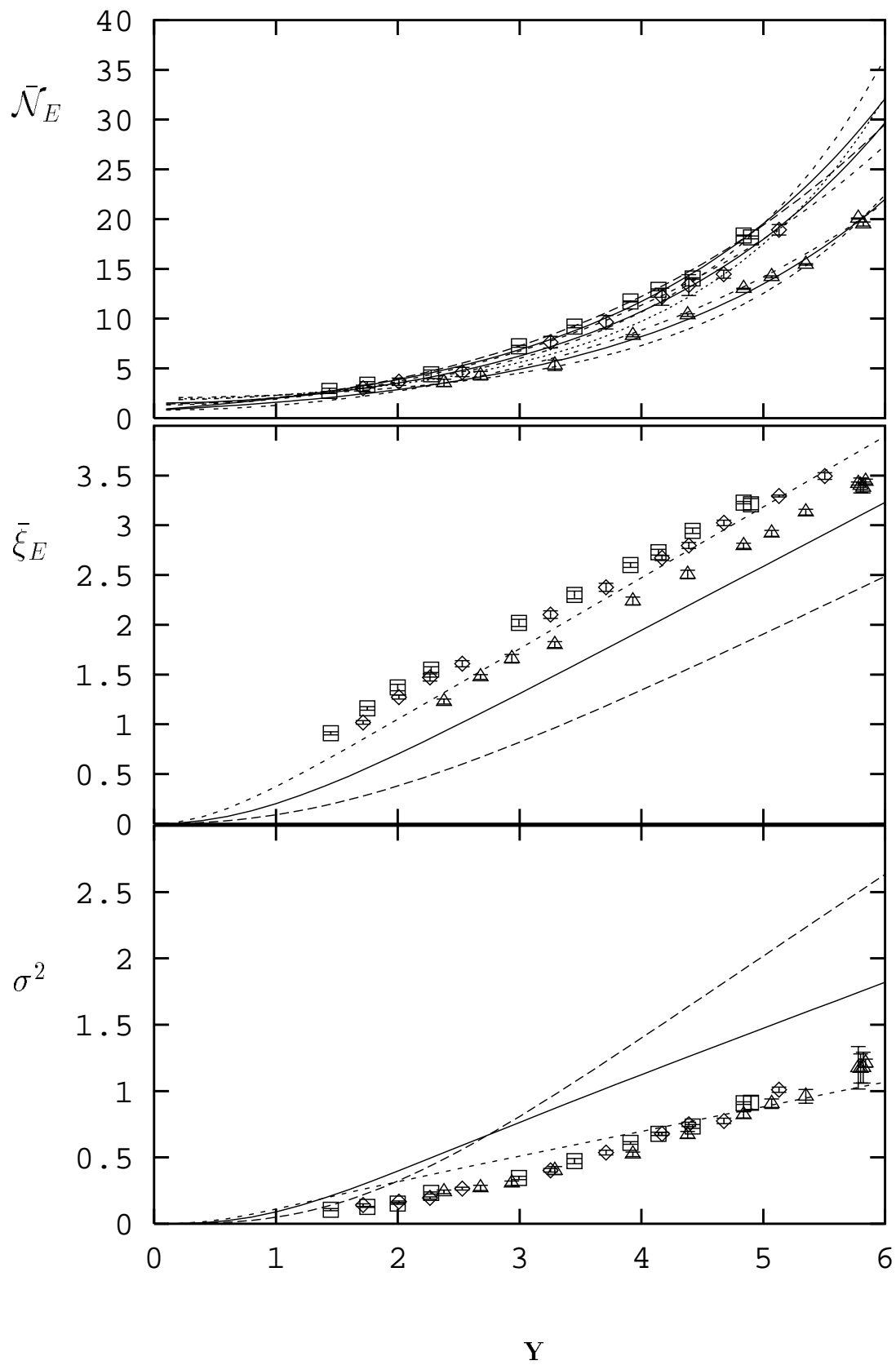


Figure 3:

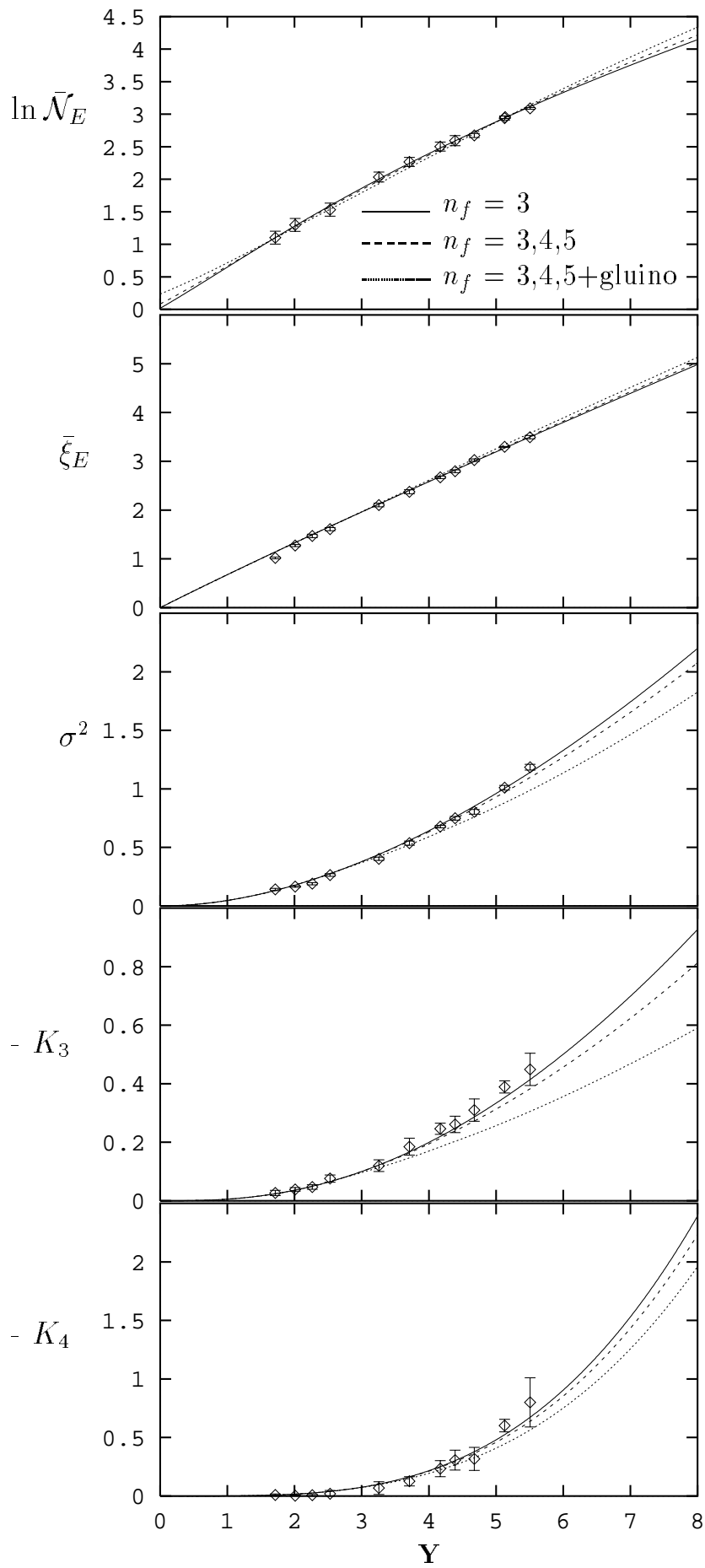


Figure 4:

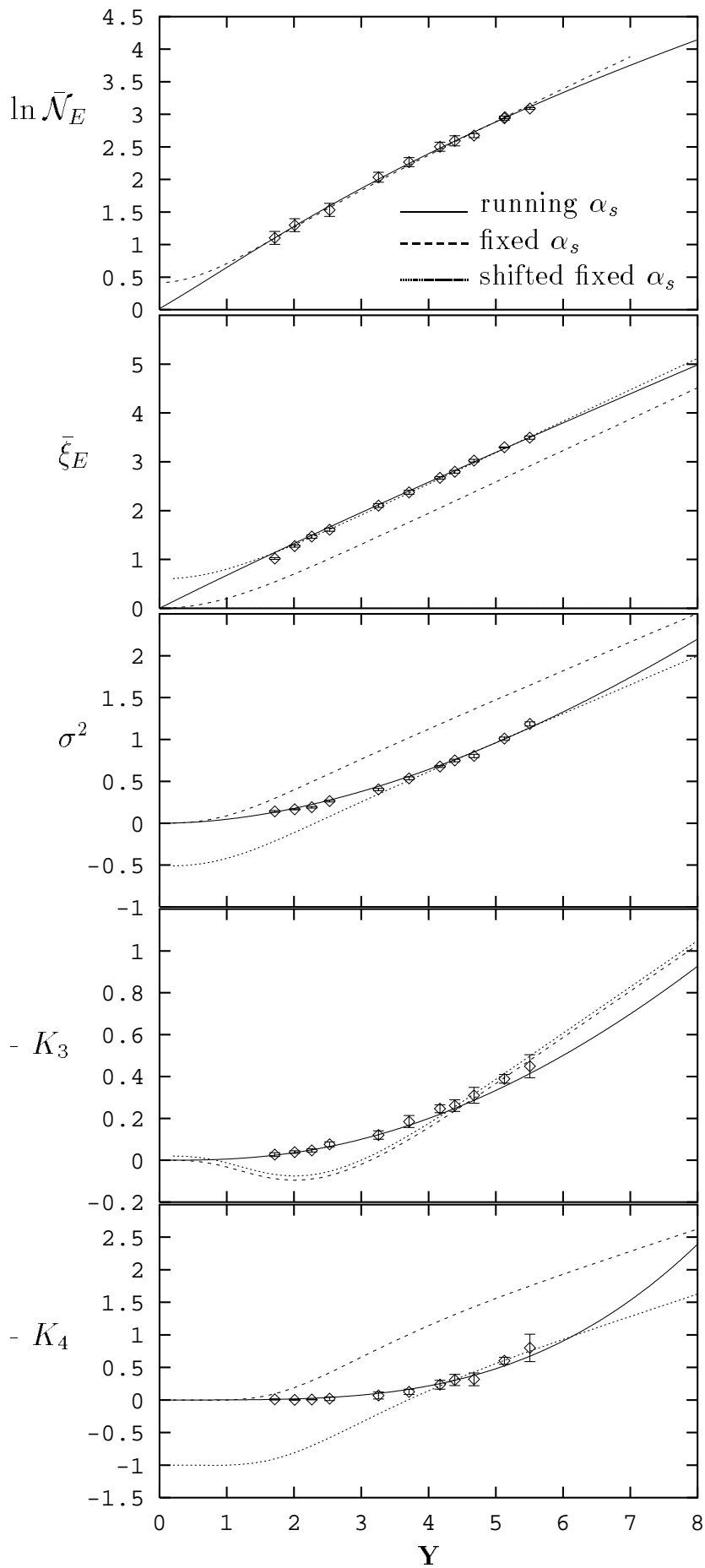


Figure 5:

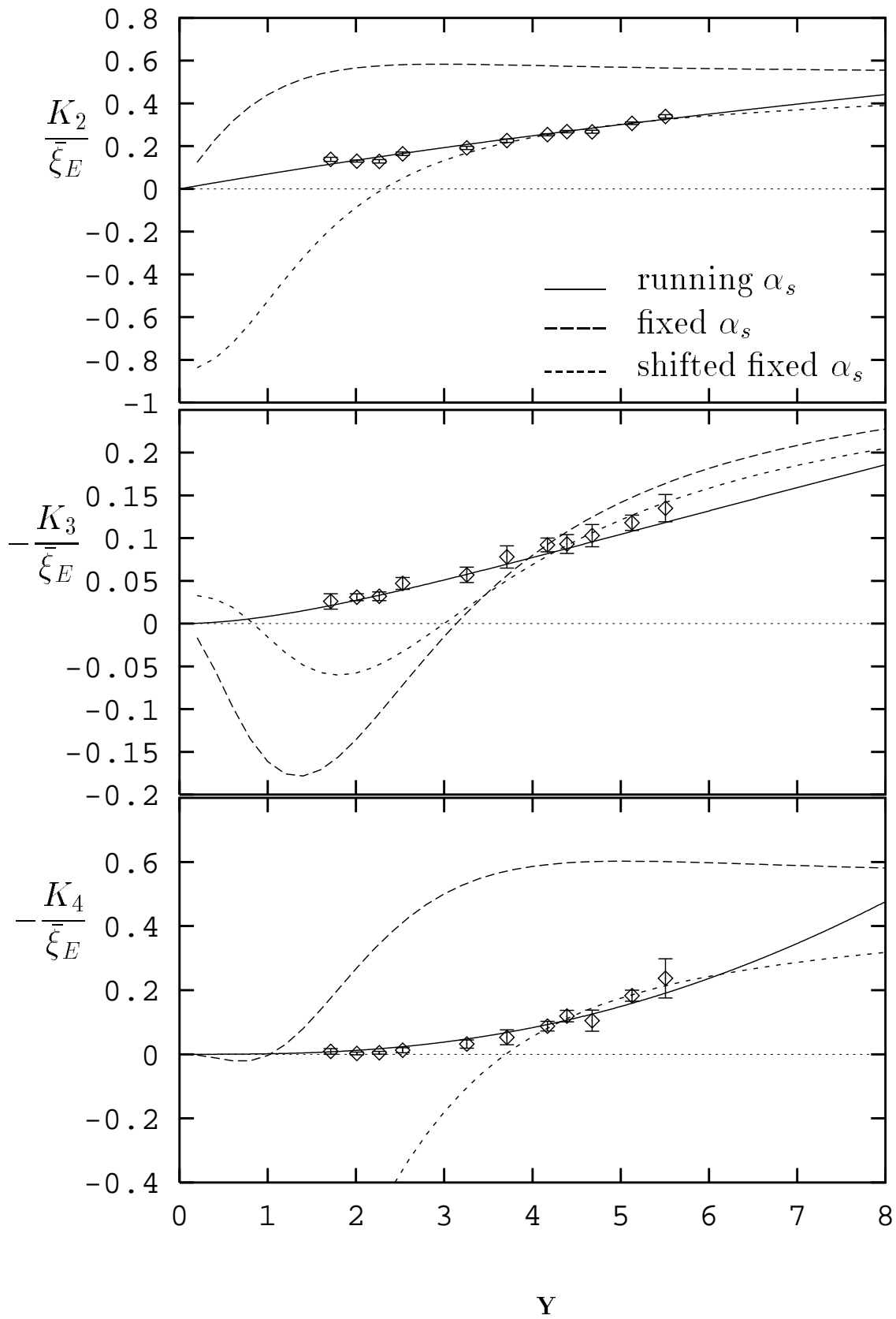


Figure 6:

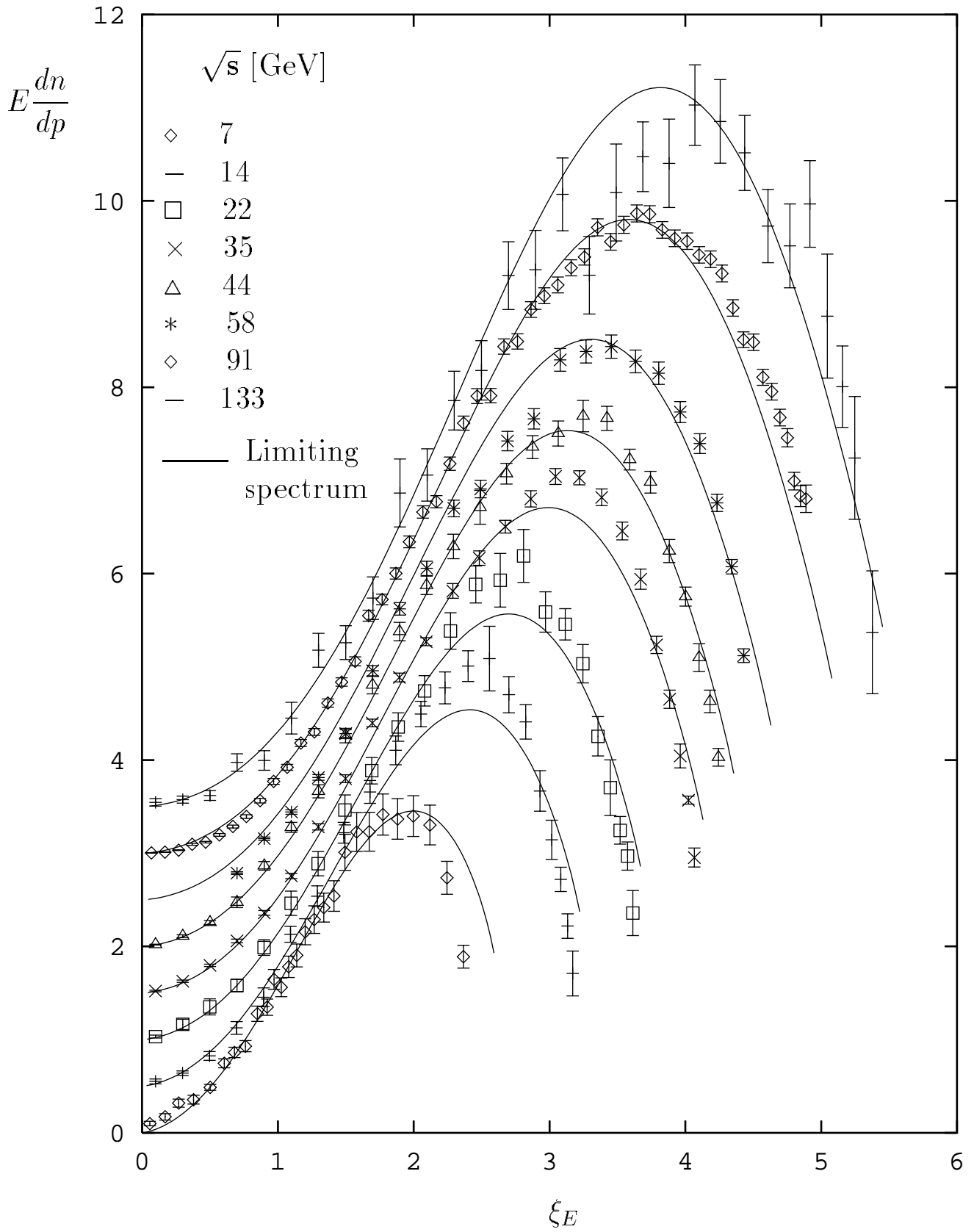


Figure 7:
40

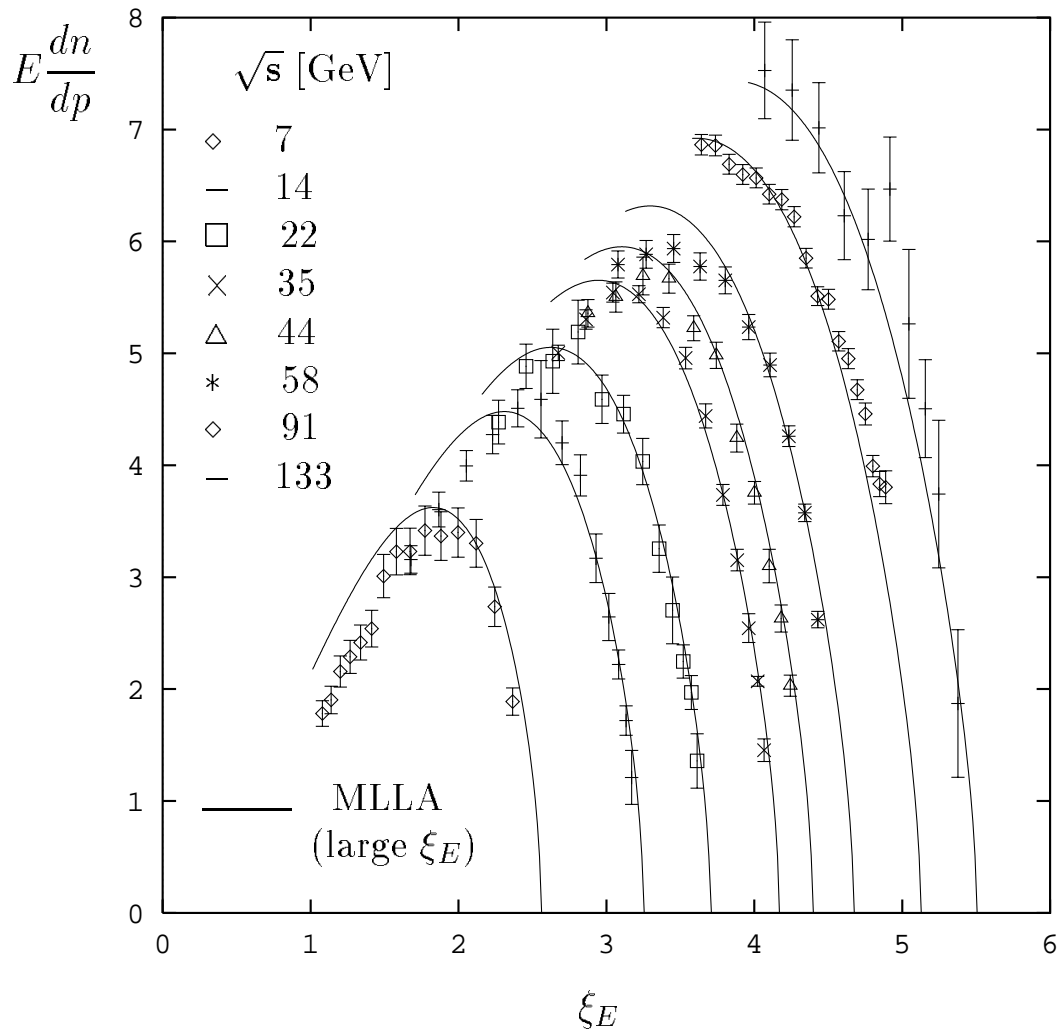


Figure 8:
41

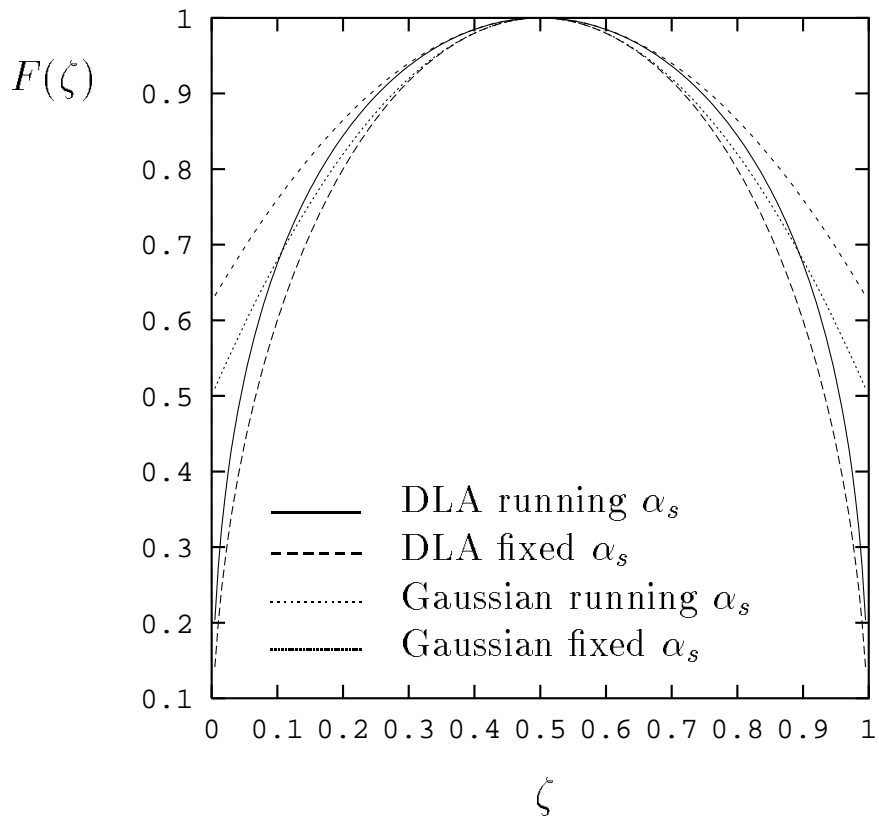


Figure 9:

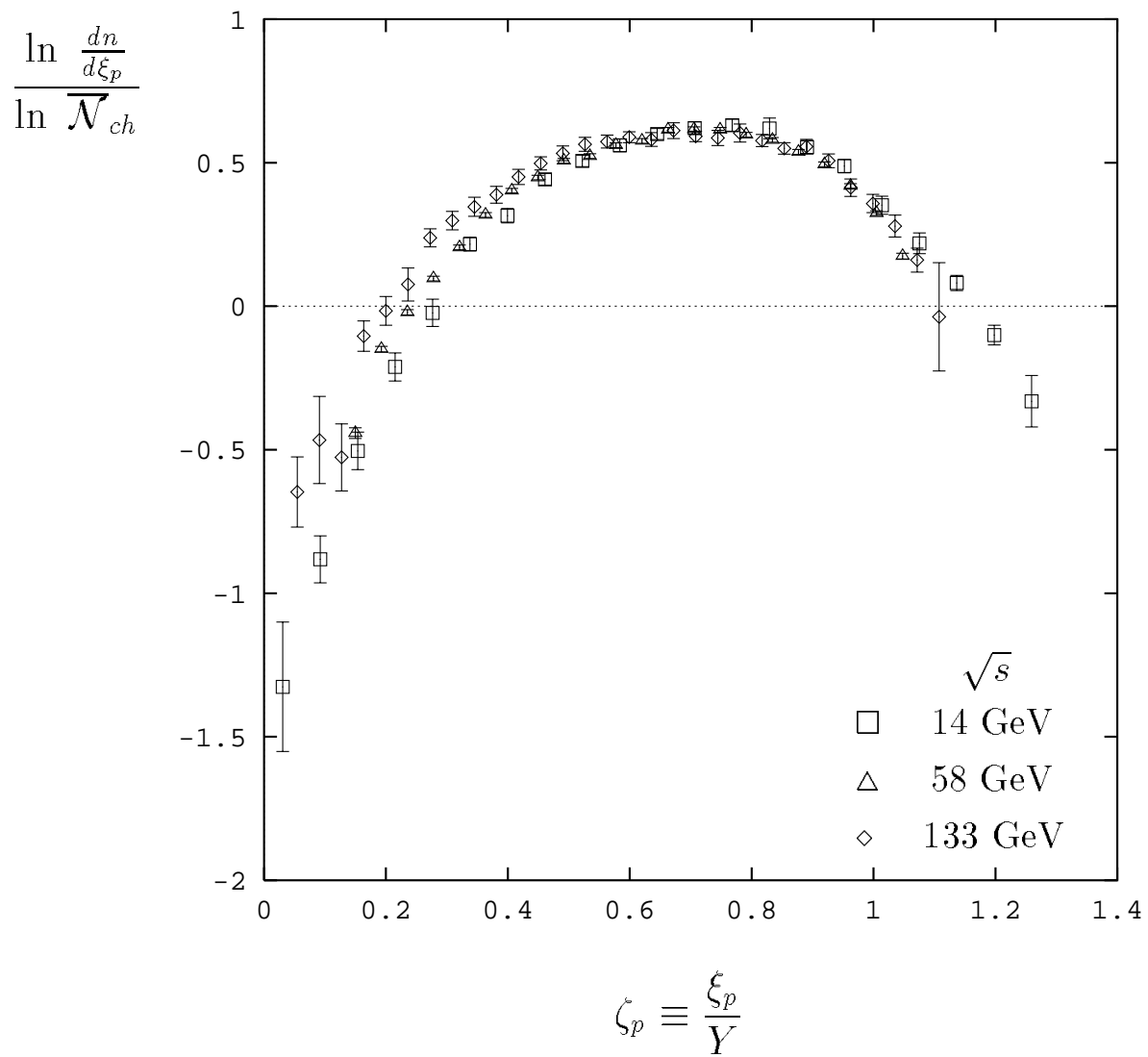


Figure 10:

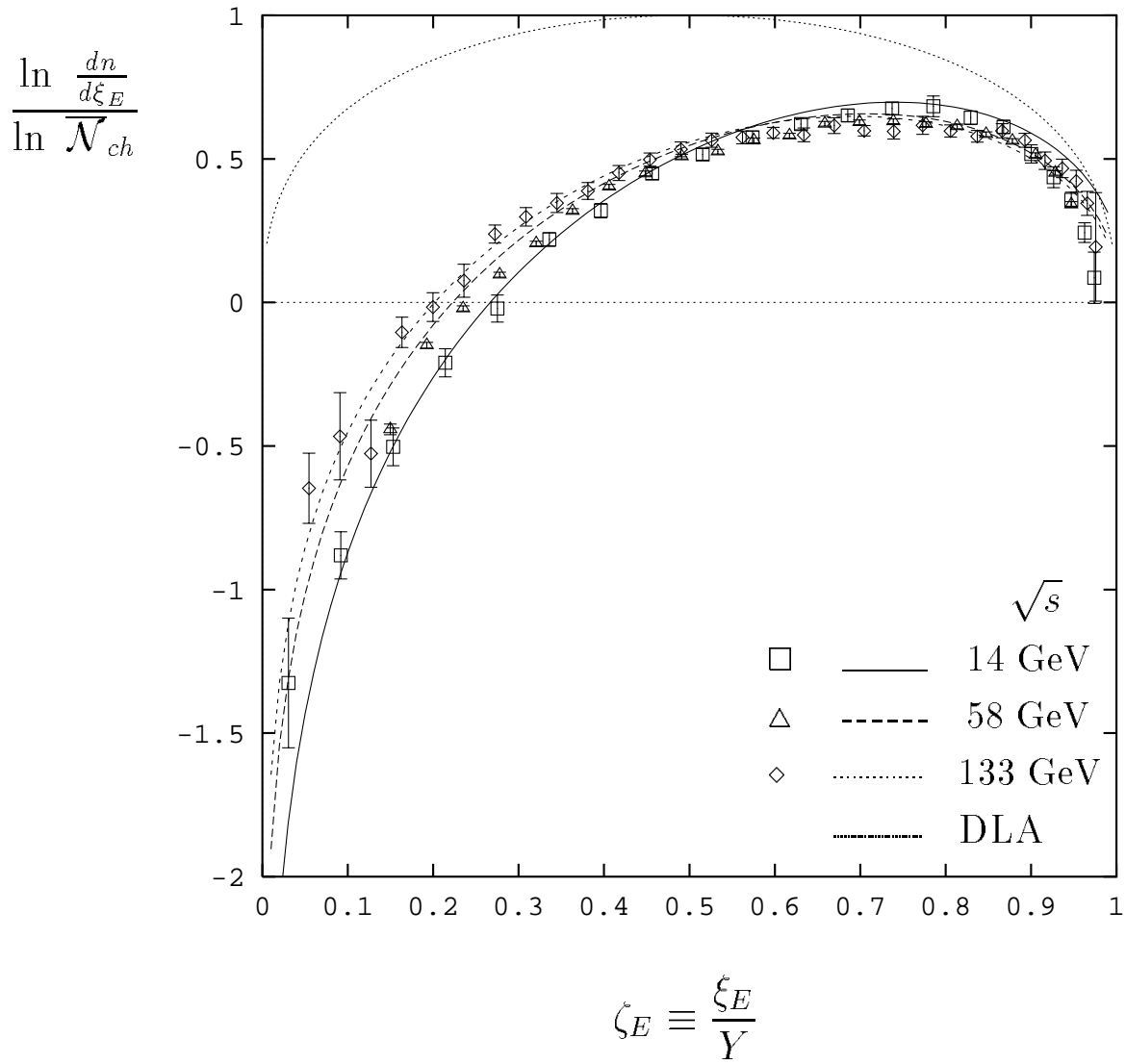


Figure 11:

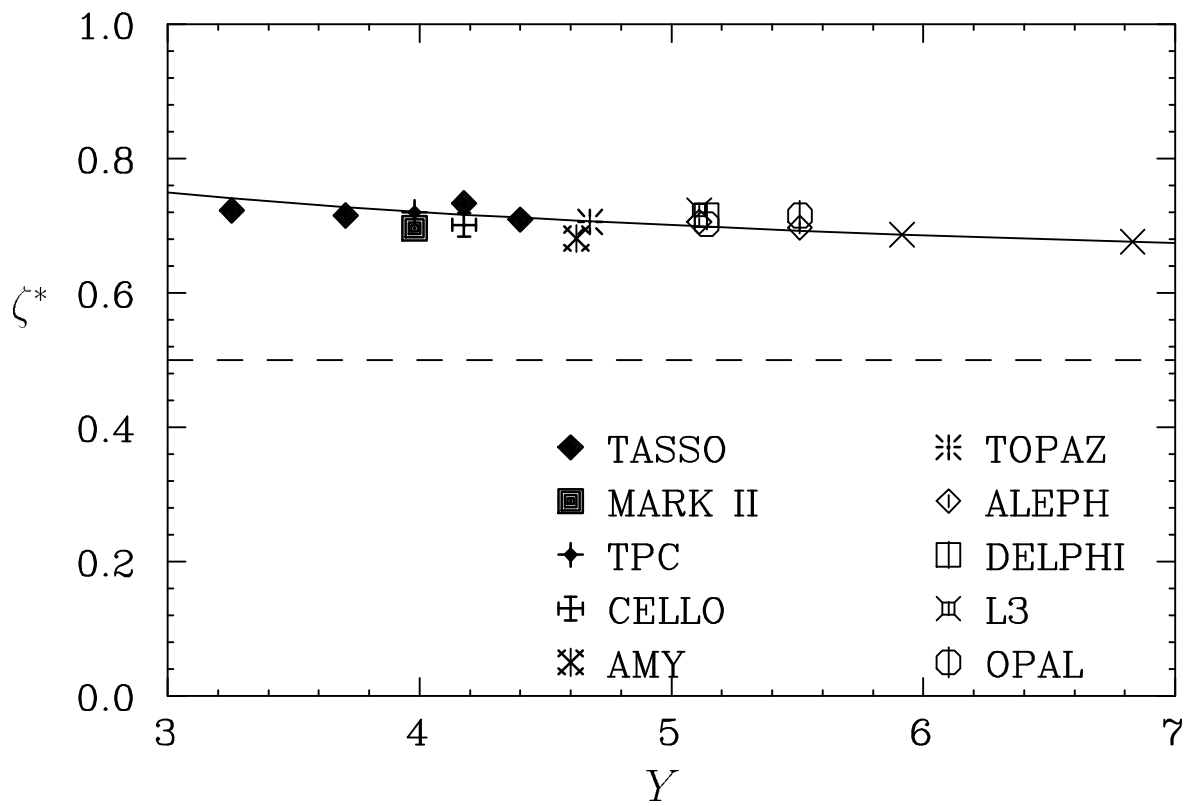


Figure 12: